FOSSIL

DOE/PC/90005-T54
(DE92002585)

LIQUID PHASE METHANOL LAPORTE PROCESS DEVELOPMENT UNIT: MODIFICATION, OPERATION, AND SUPPORT STUDIES

Topical Report for the Period April 9, 1987–March 31, 1991

Task 3.5: Development of Fundamental Rate Models for Methanol Synthesis in a Slurry Reactor

March 11, 1991

Work Performed Under Contract No. AC22-87PC90005

For
U.S. Department of Energy
Pittsburgh Energy Technology Center
Pittsburgh, Pennsylvania

By
Air Products and Chemicals, Inc.
Allentown, Pennsylvania

and

Chem Systems, Inc.
Tarrytown, New York

DOE/PC/90005--T54

DE92 002585

LIQUID PHASE METHANOL LAPORTE PROCESS DEVELOPMENT UNIT: MODIFICATION, OPERATION, AND SUPPORT STUDIES

Topical Report

Task 3.5: Development of Fundamental Rate Models for Methanol Synthesis in a Slurry Reactor

Contractor

AIR PRODUCTS AND CHEMICALS, INC.
Allentown, PA 18195

and

Subcontractor to Air Products

CHEM SYSTEMS INC.
Tarrytown, NY 10591

11 March 1991

Prepared for the United States Department of Energy
Under Contract No. DE-AC22-87PC90005
Contract Period 9 April 1987 – 31 March 1991

Contents

LIST OF TABLES

LIST OF FIGURES

LIST OF FIGURES
(continued)

Page

ABSTRACT

In support of the DOE-sponsored Liquid Phase Methanol research and development program (Contract No. DE-AC22-87PC90005), rate expressions for methanol synthesis from syngas in a slurry reactor have been developed. These rate models, which express methanol rate as a function of gas phase fugacities, were fit to the 250°C laboratory experimental data bases for two BASF methanol synthesis catalysts, S3-85 and S3-86. In addition, the S3-86 experimental data base was expanded by obtaining data on the Great Plains syngas feed. The best fit rate expressions identified for each catalyst differ in mathematical form, but were both derived from a reaction mechanism that assumes that CO and CO_2 are hydrogenated in parallel on separate sites on the surface of the catalyst. Model S3-T2, the best model identified for S3-85, yielded an average prediction error per experimental observation of 12.9%, while the average error for model XX14, the best model for S3-86, was 15.3%. Agreement between experimentally observed trends and model predictions is generally good, though some deficiencies of the models have been identified.

INTRODUCTION

The Liquid Phase Methanol (LPMEOH) process is an efficient method of producing methanol from coal-derived synthesis gas. In the LPMEOH reactor, the methanol synthesis catalyst, in a powder form, is suspended in an inert liquid medium. Because of the superior heat transfer characteristics of this slurry medium, the highly exothermic and equilibrium-limited methanol synthesis reaction can be run under essentially isothermal conditions. This enables the use of unshifted feed gases which contain high levels of CO and the achievement of a high per-pass conversion.

Successful application and optimization of the LPMEOH process requires a method of predicting methanol synthesis rate as a function of reaction conditions. A key requirement is the development of an accurate kinetic model, i.e., a mathematical expression of the intrinsic methanol synthesis rate as a function of pressure, temperature, and gas composition. A rate expression derived from fundamental considerations of the elementary steps of the reaction mechanism is desirable, because such an expression is likely to be applicable over a wide range of reaction conditions.

Historically, methanol synthesis from syngas has been one of the most studied reactions, as indicated by the extensive literature. Numerous reaction schemes and rate expressions have been developed to describe the methanol rate for a variety of reaction conditions. Most associated experimental measurements of rate have involved synthesis in packed bed reactors with high H_2/CO feed. Many of the proposed rate expressions lack important features, such as the influence of CO_2 and the water-gas shift reaction. Some of these rate models are also quite complicated and difficult to use.

The primary goal of this work was to develop a simple, fundamental rate model for slurry-phase methanol synthesis from coal-derived syngas. Development of an accurate model will assist in successful scale up and commercial implementation of the LPMEOH process.

OBJECTIVES

The objectives of the present work can be divided into three parts. The first objective was to develop a best-fit model for the older methanol synthesis catalyst (BASF S3-85) data base. At the time that this work commenced (June 1989), the BASF S3-85 data base contained many rate measurements accumulated over a few years. The newer catalyst (BASF S3-86) data base, at that time, contained only a few observations and did not include a broad range of conditions. Thus, a second objective of this work was to expand the BASF S3-86 data base to include more rate observations over a broader range of conditions. Finally, after expansion of the BASF S3-86 data base, the third objective was to develop a rate expression to describe this data base. This would include the application of rate expressions developed for the BASF S3-85 catalyst, as well as new models.

SAFETY

The major safety concerns in the experimental part of this study were the flammability of H_2 and the toxicity and flammability of CO, both of which are present in syngas. The primary measures taken to minimize the consequences of an unexpected release of these gases were: the apparatus was housed in a continuously ventilated walk-in hood, the atmosphere in the hood and the laboratory area was continuously monitored by flammable gas and CO detectors, and the flammable gas and CO detectors were interfaced to an automatic gas flow shutdown system.

ACKNOWLEDGMENT

The author would like to thank the following people who are largely responsible for obtaining the experimental data that comprises the data bases used in the modelling: T. A. Dahl, R. C. Blum, S. E. Gaul, B .L. Bhatt, T. H. Hsiung, and J. J. Lewnard.

EXPERIMENTAL

Materials:

The catalysts used for these experiments were BASF S3-85-44 and BASF S3-86-43 (previously designated F21/0E75-44 and F21/0E75-43), respectively. Hereinafter, BASF S3-85-44 and BASF S3-86-43 will be referred to as S3-85 and S3-86, respectively. Both catalysts are commercial Cu/ZnO/Al_2O_3 methanol synthesis catalysts which differ in the relative proportions of Cu, ZnO, and Al_2O_3. S3-85 is the older catalyst; S3-86 replaced S3-85 as the preferred catalyst for the process because it has shown a higher methanol synthesis rate for CO-rich syngas. The slurrying liquid used was either Witco 70 or Penreco Drakeol 10, both of which are white mineral oils.

Premixed gases, supplied from cylinders or a tube trailer, were obtained from Air Products Specialty Gases. Table A-1 of Appendix A shows the nominal compositions for the syngas mixtures. The gas compositions were chosen to simulate the bulk syngas product from various coal gasifiers, including Shell, Texaco, and Dow. In addition, two high H_2/CO gas mixtures were used. One mixture simulated the shifted syngas from the Great Plains gasification facility. The composition of the other high H_2/CO mixture, designated "balanced" gas, was such that $H_2/(CO+1.5CO_2)=2$, thereby having hydrogen and carbon oxides present in stoichiometric proportions for methanol synthesis from CO and CO_2. Also, additional syngas mixtures were used, the compositions of which simulated the removal or addition of CO_2 from the basic syngas matrices shown in Table A-1. In some experiments using the S3-85 catalyst, H_2O was added to the feed. The trace components usually present in actual coal gasifier product streams, e.g. sulfur compounds, were not present in these gas mixtures.

Experimental Apparatuses:

The data which comprise the data bases were obtained using three experimental apparatuses. A flow schematic for a typical apparatus is shown in Figure 1. The reactors used were stirred autoclaves, manufactured by Autoclave Engineers, with internal volumes of 50cc, 300cc, or 1000cc. Feed gas from cylinders or a tube trailer was compressed by a gas booster pump. Gas flow rate to the reactor was controlled by an electronic mass flow controller. The vapor product stream was passed through

FIGURE .1: Schematic of Reactor System

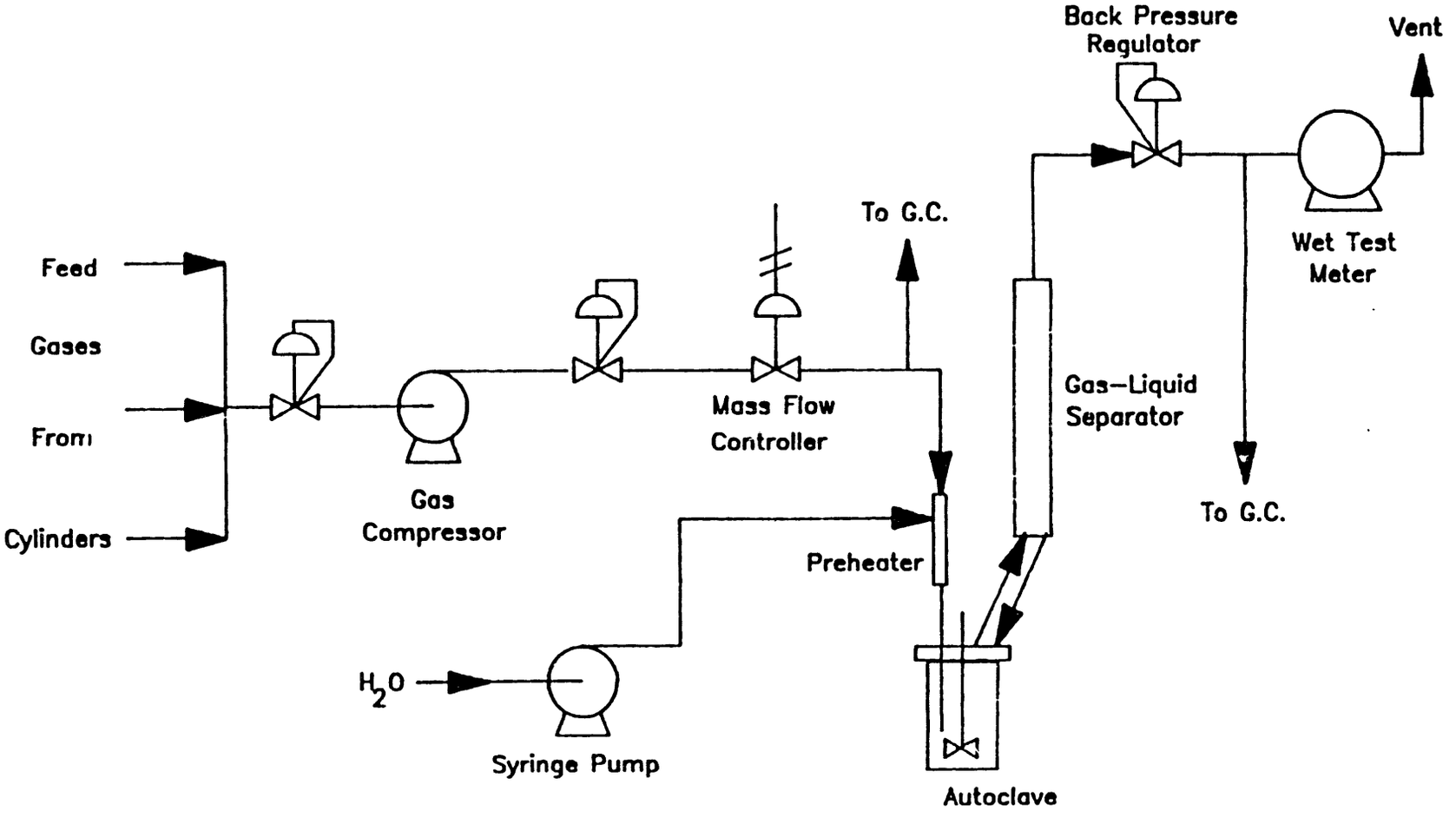

a gas-liquid separator to remove entrained and vaporized oil from the reactor. The gas-liquid separator, the heat-traced lines downstream of the reactor, and the line to the gas chromatograph were maintained at a temperature sufficient to prevent the condensation of product CH_3OH. Reactor pressure was regulated by means of a back pressure regulator and product gas flow rate was measured using a wet test meter.

For some of the experiments, H_2O was added to the feed as steam. This was done using a syringe pump which injected liquid H_2O to a feed preheater located immediately upstream of the reactor inlet. The feed preheater, an electrically-heated vessel packed with brass machine screws, vaporized the injected liquid H_2O into the feed gas stream.

The influence of mass transfer on the measured methanol rate was shown to be negligible by observing the effect of stirrer speed on the rate for each reactor. The results of these measurements indicated that, for all three reactor sizes, mass transfer influence was negligible for stirrer speeds greater than or equal to 1200 rpm. A stirrer speed of at least 1200 rpm was used for all of the data in the data bases. Since mass transfer limitations are negligible, the autoclave reactors are regarded as continuous stirred tank reactors (CSTRs). Thus, the gas phase composition in the reactor, which is equal to the effluent gas composition, determines the rate of methanol synthesis. In fitting the experimental data, the observed methanol rates were regressed on the reactor effluent fugacities calculated from effluent concentrations.

Feed and product gas compositions were measured on-line by a GC equipped with thermal conductivity detectors. Since the GC columns used did not perform well for H_2O at low concentrations, accurate quantitative analysis for H_2O was not possible. Thus, reactor effluent water concentrations are not, unfortunately, included in the data base. Water concentrations were calculated by assuming that the water-gas shift reaction was at equilibrium, as will be discussed later.

Data Bases:

Tables A-2 and A-3 of Appendix A are summaries of the laboratory autoclave data bases used in the model development for the S3-85 and S3-86 catalysts, respectively. Brief study of the limited range of reaction conditions in these data bases elucidates the fact that the experiments were not chosen for the sole purpose of developing a rate model. In fact, most of the data were obtained using practical conditions of temperature, pressure, flow rate, and gas composition. Practical conditions span a somewhat limited range of conditions, making it more difficult to adequately test the validity of a model. Of course, a model which accurately describes all practical conditions is obviously very useful.

For the S3-85 catalyst, the majority of the experiments were done using the Texaco gas matrix. Limited data for "balanced" gas and Shell gas are also included. The overwhelming majority of this data was obtained using a reaction temperature of 250°C and reaction pressure of 52.02 atm (750 psig). Thus, the S3-85 data base is somewhat limited in scope. Most of the Texaco gas data was obtained during the study of the effects of CO_2 in Texaco gas, Subtask 3.2 of the current DOE contract. Much of this data was obtained using a gas-hourly space velocity (GHSV) of 5,000 or 10,000 std.lit./kg-hr. The rightmost column of Table A-2 indicates the feed CO_2 and/or H_2O levels for experiments in which these levels were varied from the basic syngas matrix. In total, the S3-85 data base consists of 128 observations at 84 different conditions. The portion of the data base which

includes runs at 250°C consists of 112 observations at 69 different conditions of feed gas composition and GHSV.

In contrast to the S3-85 data base, the S3-86 data base spans a considerably broader range of conditions and is not as concentrated on the Texaco gas matrix. Table A-3 shows that the experimental runs are fairly evenly divided among the Texaco, Dow, and Great Plains gas matrices. Broader ranges of GHSV and pressure are also a feature of the S3-86 data base. The inclusion of extensive runs on Great Plains gas, including the effect of feed CO_2, enables the fitting and testing of models at H_2-rich feed conditions. However, in contrast to the S3-85 data base, the S3-86 data base does not include any runs in which H_2O was added to the feed, nor does it include any data on the very CO-rich Shell gas. In total, the S3-86 data base consists of 85 observations at 57 different conditions. The portion of the data base which includes runs at 250°C consists of 61 observations at 52 different conditions of feed gas composition, pressure, and GHSV.

Calculations:

To enable the developed rate models to be applicable over the broadest range of reaction conditions possible, gas phase fugacities were used in the rate expressions instead of partial pressures. This required the conversion of measured reactor effluent mole fractions and reactor total pressure to fugacities for each experimental run. To do this for each data base, the relevant data were assembled into a PC-based ASCII file. The necessary data for each run for this conversion to fugacity included the temperature, total pressure, outlet mole fractions of H_2, CO, CO_2, CH_3OH, and inerts (CH_4+N_2), and methanol rate. These data were transferred serially to a file on the Air Products mainframe computer. There the data were used by a Fortran program that calculated normalized mole fractions, H_2O concentration by water-gas shift equilibrium, and, finally, fugacity coefficients and fugacities. The determination of fugacities was done using an Air Products proprietary subroutine which uses the modified Redlich-Kwong equation of state with experimentally determined parameter values. The resulting fugacities were serially downloaded from the mainframe to an ASCII format file on the PC.

For each data base a file was assembled which contained, for each run, the observation number, measured methanol rate, data weight factor, and fugacities of H_2, CO, CO_2, and CH_3OH. The data weight factor is an input to the non-linear regression package and was used to assign relative importance to the square of the residual calculated for each observation. If the data weight factor is 1.0 for all observations, each is weighted equally. Assigning a value of less than 1.0 puts less significance on that observation for the regression. Data weight factors of less than 1.0 were used in the S3-85 data base for runs using Texaco gas at 250°C and 5,000 and 10,000 GHSV, because these conditions were repeated many times experimentally.

A non-linear, least squares regression routine in SAS was used for the data regressions. An example SAS program listing is shown in Appendix B. SAS was run on a Compaq Deskpro 286 equipped with a math coprocessor. The data files containing the fugacities for each data base were converted into SAS datasets and used as input to the regression routine. Either the Marquardt or modified Gauss-Newton iterative methods were used in minimizing the residual sum of squares. The residual sum of squares, or sum of the squares of the errors (SSE), is defined as:

$$SSE = \sum_i (\text{predicted rate}_i - \text{measured rate}_i)^2.$$

For each regression, specification of initial parameter estimates and the partial derivative of the rate expression with respect to each parameter were required. The version of SAS used (version 6.03) was quite interactive and allowed for real-time observation of the convergence process. This way the iterations could be stopped if the search was headed toward unrealistic values of the parameters or got "bogged down". Convergence time was a function of the quality of the initial parameter estimates, but, for fairly good guesses, a typical 6-parameter rate expression required 5-10 minutes to converge. The results of the regression were transferred to a spreadsheet where plots that compare measured and predicted results were generated.

RESULTS AND DISCUSSION

I. Basis for Modeling:

In the development of rate expressions, emphasis was on those derived from assumed sequences of elementary steps, rather than empirical mathematical expressions. The assumed reaction mechanisms were meant to be consistent with published aspects of the chemisorption of the reacting species, observations of surface intermediates, and isotopic tracer studies. Also, investigations of the effect of reaction conditions on experimentally measured methanol rate from the published literature and from work done in Air Products laboratory, was used as additional guidance in developing rate expressions.

Previous published work provides some guidance in terms of probable reaction mechanisms. However, much controversy exists in the literature regarding the source of carbon, whether CO or CO_2, in methanol synthesis from $CO/CO_2/H_2$ mixtures. Some authors have speculated that methanol is formed largely from CO, while the primary role of CO_2 is to maintain the catalyst in the most active state [1,2]. Other authors believe that the primary carbonaceous reactant is CO_2 [3-6]. For example, workers at ICI have recently presented some rather compelling experimental evidence that methanol is formed directly from CO_2 [5,6], at least under the reaction conditions used in their studies. Indeed, other investigators believe that both CO and CO_2 hydrogenation are kinetically important in methanol synthesis [7-11]. Though universal agreement does not exist regarding the primary carbon source, general agreement exists that the presence of some CO_2 is necessary to achieve high methanol synthesis rate. In addition, the water-gas shift reaction is important under methanol synthesis conditions and frequently complicates the interpretation of experimental results.

Noteworthy is the fact that many of the studies referred to above involved methanol synthesis from H_2-rich syngas, i.e., syngas representative of that obtained from steam-methane reforming (SMR). The syngas obtained from the gasification of coal is typically much richer in carbon oxides, especially CO. Thus, the relative importance of CO and CO_2 as carbon sources may be different for coal-derived, CO-rich gas than that for SMR-derived syngas.

In view of the above, the present work is focused on rate expressions derived from reaction mechanisms in which methanol is formed from both CO and CO_2 hydrogenation. This generality will allow the data fit to decide which route allows for a better description of the experimental data. However, a cautionary note is required here. The validation of a reaction mechanism by means of best fit rate expressions is tenuous, at best. In other words, if a rate model fits the data best, this alone does not provide sufficient evidence that the model is accurate. This is true largely because

vastly different reaction mechanisms may yield very similar rate expressions. Other corroborating experimental and, perhaps, theoretical evidence is required to adequately validate a reaction mechanism.

Assuming that methanol is produced from CO and CO_2 hydrogenation, the relevant stoichiometric equations are:

$$CO + 2H_2 \text{ <====> } CH_3OH \qquad [1]$$

$$CO_2 + 3H_2 \text{ <====> } CH_3OH + H_2O \qquad [2]$$

Occurring along with these reactions is the water-gas shift (WGS) reaction:

$$CO + H_2O \text{ <====> } CO_2 + H_2 \qquad [3]$$

Note that only two of these three equations [1-3] are algebraically independent because each can be written as a linear combination of the other two.

In the present work, the development of rate expressions from assumed sequences of surface reaction steps has been done using standard Langmuir-Hinshelwood kinetics, probably the most commonly used technique because of its relative simplicity. A number of simplifying assumptions are intrinsic in analysis by the Langmuir-Hinshelwood method in order to make the derivation mathematically tractable and produce an explicit, analytic expression for the rate. As a review, some of the assumptions inherent in this technique are:

(1) The reactants, intermediates, and products adsorb on discrete, energetically homogeneous sites on the surface of the catalyst.

(2) Chemisorption is confined to a monolayer.

(3) The fractional coverage by reaction intermediates is negligible relative to the coverage by reactants and products.

(4) One step in the reaction pathway is the rate-determining step (RDS).

(5) Steps in the reaction pathway which are not rate limiting are at equilibrium.

The Langmuir-Hinshelwood treatment generally produces a fractional rate expression in terms of the partial pressures or fugacities of the reactants and products. The numerator has a forward and a reverse reaction term, while the denominator consists of a sum of adsorption terms for the reactants and products. The assumption of a particular RDS influences the form of the numerator. The denominator is dictated entirely by the chemisorption of the reactants and products and is not influenced by the RDS, provided the adsorption of a reactant or desorption of a product is not the RDS.

As mentioned earlier, the majority of the experimental observations in the S3-85 and S3-86 data bases were done using a reaction temperature of 250°C. In fact, relatively few runs were done at temperatures other than 250°C, especially for the S3-85 data base. In view of this, the work here was confined to the development of rate expressions for methanol synthesis at 250°C. However, as will be apparent in the derivation of the models, each parameter is typically a product of rate and adsorption equilibrium constants, both of which are exponential functions of temperature. Thus, a rate expression explicit in temperature would have twice the number of parameters as the isothermal one. The determination of the additional parameters for the non-isothermal rate expressions had to be left to future work.

Ranking of the quality of the rate expressions was done by considering two basic criteria. Firstly, the sum of the squares of the residuals was used to judge the quality of the fit. Secondly, the rate expressions were judged in their accuracy in describing experimentally observed trends, for example, the effect on the methanol rate of gas-hourly space velocity (GHSV), feed CO_2 content, etc.

The results will be presented in three parts. First, the development and testing of rate expressions for the S3-85 data base will be discussed. Second, experimental results which expanded the data base for S3-86, consisting largely of additional runs for the H_2-rich Great Plains gas matrix, will be presented. Third, and perhaps most importantly, modeling of the S3-86 data base will be discussed. As mentioned previously, the S3-86 data base is distributed more equitably over a broader range of gas composition, gas-hourly space velocity, and total pressure than the S3-85 data base. Thus, the S3-86 data base provides a much more demanding test of a general model. In fact, rate expressions which best fit the S3-85 data base are not the best for the S3-86 data base.

II. Modeling of S3-85 Catalyst Data Base:

Rate expressions were derived primarily by using variations of the basic reaction mechanism of Graaf et al.[9]. Graaf et al. have assumed that CO and CO_2 are hydrogenated in parallel on the surface. Hydrogenation of each takes place by simple, stepwise addition of hydrogen atoms, formed by the dissociative adsorption of H_2, until gaseous product CH_3OH is produced. Graaf et al. have also assumed that there are two types of sites: CO and CO_2 adsorb competitively on site 1 (denoted s1), while H_2 and H_2O adsorb competitively on site 2 (denoted s2). The adsorption of product CH_3OH is assumed to be negligible. So, the first steps in this mechanism are the adsorption of CO, CO_2, and H_2:

$$CO(g) + s1 = CO\text{-}s1 \quad [4]$$
$$CO_2(g) + s1 = CO_2\text{-}s1 \quad [5]$$
$$H_2(g) + s2 = 2H\text{-}s2 \quad [6]$$

Methanol is produced from CO by stepwise hydrogenation:

$$CO\text{-}s1 + H\text{-}s2 = HCO\text{-}s1 + s2 \quad [7]$$
$$HCO\text{-}s1 + H\text{-}s2 = H_2CO\text{-}s1 + s2 \quad [8]$$
$$H_2CO\text{-}s1 + H\text{-}s2 = H_3CO\text{-}s1 + s2 \quad [9]$$
$$H_3CO\text{-}s1 + H\text{-}s2 = CH_3OH(g) + s1 + s2 \quad [10]$$

In parallel, methanol is also produced from CO2, by stepwise hydrogenation:

$$CO_2\text{-}s1 + H\text{-}s2 = HCO_2\text{-}s1 + s2 \quad [11]$$
$$HCO_2\text{-}s1 + H\text{-}s2 = H_2CO_2\text{-}s1 + s2 \quad [12]$$
$$H_2CO_2\text{-}s1 + H\text{-}s2 = H_3CO_2\text{-}s1 + s2 \quad [13]$$
$$H_3CO2\text{-}s1 + H\text{-}s2 = H_2CO\text{-}s1 + H_2O\text{-}s2 \quad [14]$$

$$H_2CO\text{-}s1 + H\text{-}s2 = H_3CO\text{-}s1 + s2 \quad [15]$$
$$H_3CO\text{-}s1 + H\text{-}s2 = CH_3OH(g) + s1 + s2 \quad [16]$$
$$H_2O\text{-}s2 = H_2O(g) + s2 \quad [17]$$

Graaf et al. have also considered the kinetics of the water-gas shift reaction. As mentioned earlier, for the present work, lack of experimental measurements of exit water concentration made regression on the rate of water formation impossible. Instead, the water-gas shift reaction was assumed to be at equilibrium in the present work and the water concentration was calculated using this assumption.

Graaf et al. derived Langmuir-Hinshelwood rate expressions for methanol synthesis from this mechanism [9]. The hydrogenation of CO and CO_2 were assumed to occur independently but in parallel, even though some of the elementary reactions are the same. Thus, CO and CO_2 hydrogenation each yield a term in the rate expression, but share the same denominator. The numerator terms, or "driving force" groups, for each term depend on the choice of RDS. The assumed RDS and corresponding driving force group appearing in the numerator of the rate expression for CO and CO_2 hydrogenation are:

RDS	CO Hydrogenation Driving Force Group
[7]	$f_{CO}f_{H2}^{1/2} - f_{CH3OH}/(K_1 f_{H2}^{3/2})$
[8]	$f_{CO}f_{H2} - f_{CH3OH}/(K_1 f_{H2})$
[9]	$f_{CO}f_{H2}^{3/2} - f_{CH3OH}/(K_1 f_{H2}^{1/2})$
[10]	$f_{CO}f_{H2}^{2} - f_{CH3OH}/(K_1)$.

RDS	CO2 Hydrogenation Driving Force Group
[11]	$f_{CO2}f_{H2}^{1/2} - f_{CH3OH}f_{H2O}/(K_2 f_{H2}^{5/2})$
[12]	$f_{CO2}f_{H2} - f_{CH3OH}f_{H2O}/(K_2 f_{H2}^{2})$
[13]	$f_{CO2}f_{H2}^{3/2} - f_{CH3OH}f_{H2O}/(K_2 f_{H2}^{3/2})$
[14]	$f_{CO2}f_{H2}^{2} - f_{CH3OH}f_{H2O}/(K_2 f_{H2})$

[15] $f_{CO2}f_{H2}^{5/2}/f_{H2O} - f_{CH3OH}/(K_2 f_{H2}^{1/2})$

[16] $f_{CO2}f_{H2}^{3}/f_{H2O} - f_{CH3OH}/K_2$

Here, K_1 and K_2 are the equilibrium constants for reactions [1] and [2], respectively. The denominator, or adsorption terms, for the rate expressions are $(1+K_{CO}f_{CO}+K_{CO2}f_{CO2})$ for site s1 and $(1+K_{H2}^{1/2}f_{H2}^{1/2}+K_{H2O}f_{H2O})$ for site s2. These terms are a product in the denominator of the rate expression since each possible RDS involves participation of s1 and s2.

Rate expressions from the mechanism of Graaf et al. were fit to the S3-85 250°C data base. Before fitting the data base, the expression $f_{H2O}=f_{CO2}f_{H2}/(K_{WGS}f_{CO})$ was used to eliminate f_{H2O} in the rate expressions to reflect the assumption of equilibrium for the water-gas shift reaction. Use was also made of the fact that $K_2=K_1/K_{WGS}$.

The best fit for the Graaf et al. mechanism was obtained for the rate expression derived assuming that step [9] for CO hydrogenation and step [12] for CO_2 hydrogenation are the RDSs for methanol synthesis. In addition, the regressions showed that two parameters could be eliminated with negligible effect on the data fit because $K_{CO}f_{CO}+K_{CO2}f_{CO2} >> 1$ and $K_{H2}^{1/2}f_{H2}^{1/2}+K_{H2O}f_{H2O} >> 1$ in the denominator, that is, vacant sites are negligible. Thus, the number of adjustable parameters in each rate expression was reduced to four. This model, designated A3-C2, is shown in the first line of Table 1. Model A3-C2, with the best-fit parameters shown in Table 1, has a residual sum of squares of 1,170 gmol/kg-hr, which corresponds to an average absolute error of 13.8% per observation. The absolute error for an observation is defined as the absolute value of 100%x(predicted rate - measured rate)/(measured rate).

Also shown in Table 1 is another model, S3-T2, which fits the data base slightly better than model A3-C2. Model S3-T2 was derived from the same basic mechanism as A3-C2, with some important differences. Instead of CO and CO_2 adsorbing on the same site, each adsorbs on separate sites. In addition, H_2 adsorbs dissociatively on each of these sites. Stepwise hydrogenation occurs on each site through the same intermediates as model A3-C2. Model S3-T2 yields a residual sum of squares of 1,030 gmol/kg-hr, corresponding to an average absolute error of 12.9%.

For comparison, also shown in Table 1 is model W1, previously proposed as a viable rate expression. As can be seen, model W1 results in a much worse data fit than either A3-C2 or S3-T2, with a residual sum of squares of 5,697 gmol/kg-hr and average absolute error per observation of 31.2%. The lack of fit is not surprising since model W1 has no CO_2 dependence.

Model S3-T2 was the best model found for the S3-85 data base. A compilation of the reactor exit concentrations and calculated fugacities of H_2, CO, CO_2, and CH_3OH, the measured rate, the predicted rate, the residual, and the prediction error is shown in Table B-1 of Appendix B.

The following are some comparisons between measured and predicted methanol rates for model S3-T2. Note that the predicted rates are based on fugacities calculated from the measured reactor exit gas composition and total pressure for each run. A parity plot for this model is shown in Figure 2. Scatter about the 45° line is fairly uniform. Shown in Figures 3-10 are comparisons between measured and predicted rate trends. Figures 3 and 4 show the effect of CO_2 concentration in the Texaco gas matrix at 5,000 GHSV and 10,000 GHSV, respectively. Good agreement between

TABLE 1

Rate Expressions for S3-85 Data Base

$K_1 = f_{CH3OH}/f_{CO}(f_{H2})^2 = 0.0018\ atm^{-2}$

Model Name	Rate Expression	Parameter Values	Residual Sum of Squares (gmol/kg-hr)	Avg. Abs. Error per Observation (%)
A3-C2	$r_{CH_3OH} = \dfrac{b_0\left(f_{CO}f_{H_2}^{3/2} - \dfrac{f_{CH_3OH}}{K_1 f_{H_2}^{1/2}}\right) + b_1\left(f_{CO_2}f_{H_2} - \dfrac{f_{CH_3OH}f_{CO_2}}{K_1 f_{CO} f_{H_2}}\right)}{\left(f_{CO} + b_2 f_{CO_2}\right)\left(f_{H_2}^{1/2} + b_3\dfrac{f_{CO_2}f_{H_2}}{f_{CO}}\right)}$	b_0=0.66 gmol/(kg-hr-atm$^{5/2}$) b_1=174 gmol/(kg-hr-atm^2) b_2=5.91 atm^{-1} b_3=0.87 atm^{-1}	1170	13.8
S3-T2	$r_{CH_3OH} = \dfrac{b_0\left(f_{CO}f_{H_2}^{3/2} - \dfrac{f_{CH_3OH}}{K_1 f_{H_2}^{1/2}}\right)}{\left(f_{CO} + b_2\dfrac{f_{CO_2}f_{H_2}}{f_{CO}}\right)^2} + \dfrac{b_1\left(f_{CO_2}f_{H_2} - \dfrac{f_{CH_3OH}f_{CO_2}}{K_1 f_{CO} f_{H_2}}\right)}{\left(1 + b_3\dfrac{f_{CO_2}f_{H_2}}{f_{CO}}\right)^2}$	b_0=4.73 gmol/(kg-hr-atm$^{5/2}$) b_1=1.22 gmol/(kg-hr-atm^2) b_2=0.45 atm^{-1} b_3=0.27 atm^{-1}	1030	12.9
W1	$r_{CH_3OH} = b_0 f_{CO}^{1/3} f_{H_2}^{2/3}\left(1 - \dfrac{f_{CH_3OH}}{K_1 f_{CO} f_{H_2}^2}\right)$	b_0=1.72 gmol/(kg-hr-atm)	5697	31.2

FIGURE 2

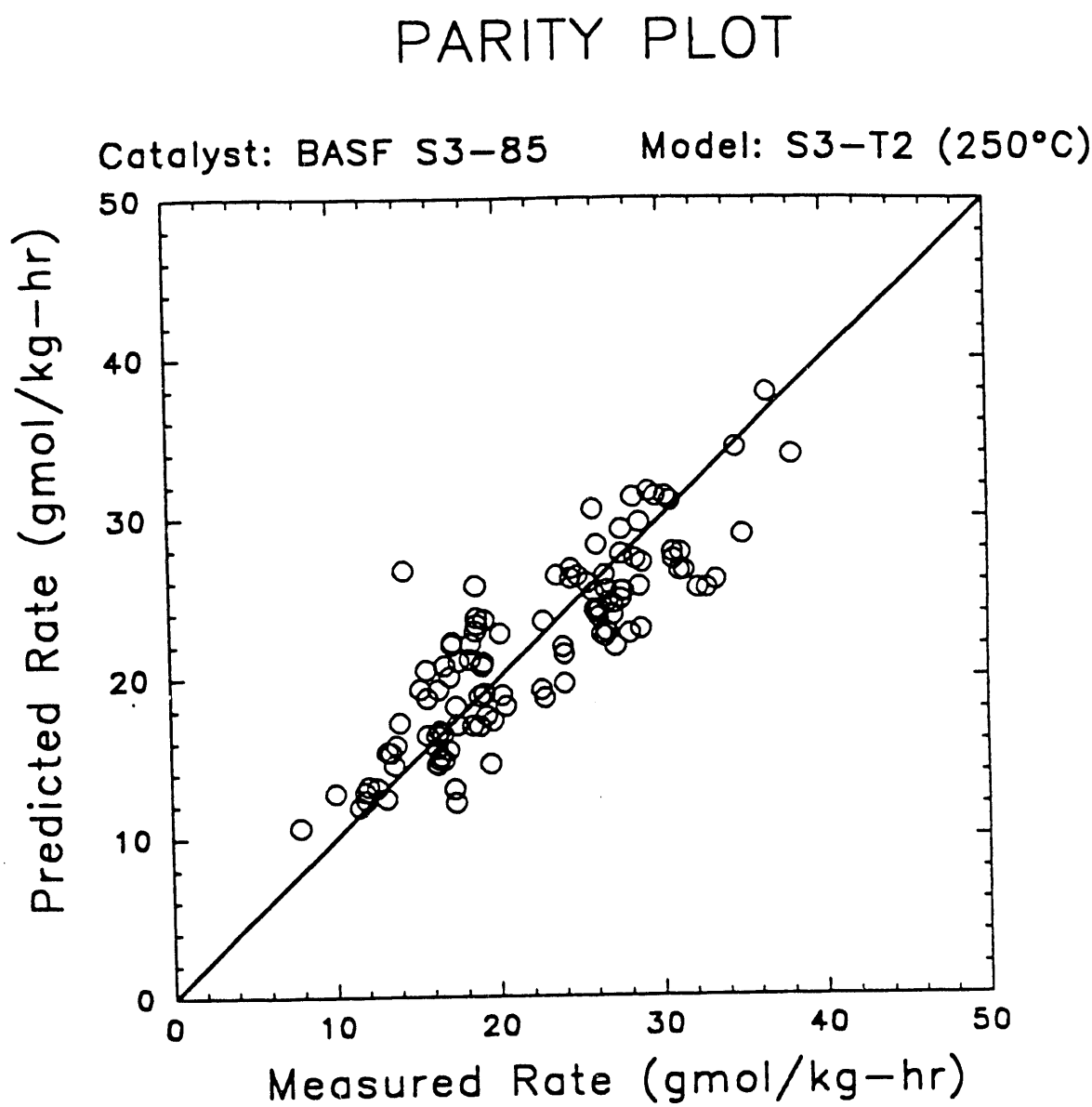
PARITY PLOT
Catalyst: BASF S3-85
Model: S3-T2 (250°C)
Predicted Rate (gmol/kg-hr)
Measured Rate (gmol/kg-hr)
0
10
20
30
40
50

FIGURE 3

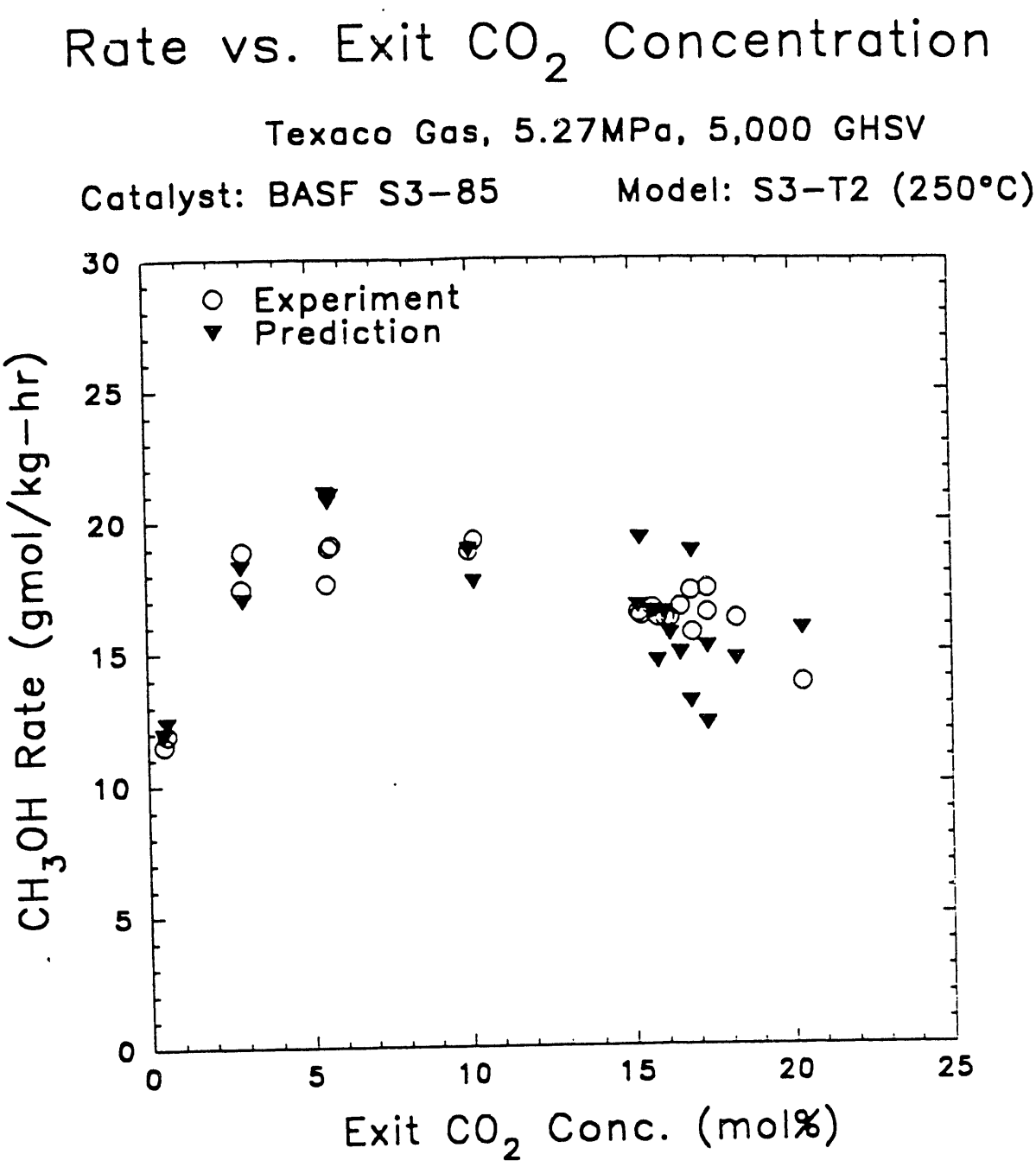
Rate vs. Exit CO_2 Concentration
Texaco Gas, 5.27MPa, 5,000 GHSV
Catalyst: BASF S3-85
Model: S3-T2 (250°C)
Experiment
Prediction
CH_3OH Rate (gmol/kg-hr)
Exit CO_2 Conc. (mol%)
0
5
10
15
20
25
30

FIGURE 4

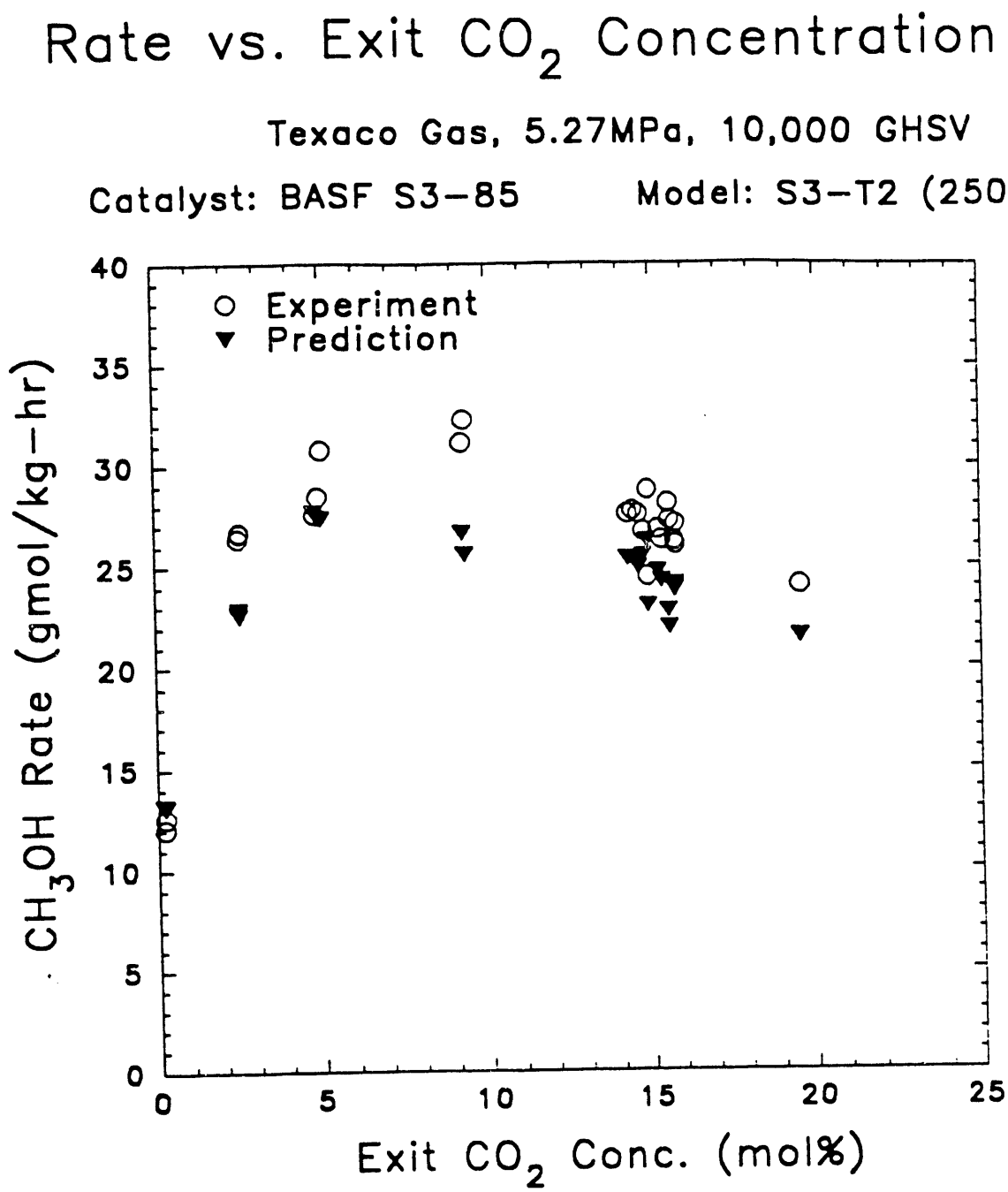
Rate vs. Exit CO_2 Concentration
Texaco Gas, 5.27MPa, 10,000 GHSV
Catalyst: BASF S3-85
Model: S3-T2 (250°C)
Experiment
Prediction
CH_3OH Rate (gmol/kg-hr)
Exit CO_2 Conc. (mol%)
0
5
10
15
20
25
30
35
40

measured and predicted is observed; as expected from the form of the rate expression, the model quite adequately predicts the trend. Figures 5 and 6 show measured and predicted rates for H_2O feed addition to Texaco gas with 0 mol% feed CO_2 at 5,000 GHSV and 10,000 GHSV, respectively. At 5,000 GHSV, it appears that the predicted increase in rate with H_2O addition is steeper than that measured. Figures 7 and 8 show measured and predicted rates for H_2O addition to Texaco gas with 13 mol% CO_2. At 10,000 GHSV, the model predicts a slight increase in rate with H_2O addition, while the experimental results indicate the opposite. Measured and predicted rates for H_2O addition to the Shell gas matrix at 5,000 GHSV and 10,000 GHSV are shown in Figures 9 and 10, respectively. Again, at 10,000 GHSV, the model predicts a steeper rise in rate with increased feed H2O concentration. The rate is somewhat overpredicted at 5,000 GHSV across the range of feed H2O concentration.

Some important points regarding characteristics of the data base which affect the quality of the fit for model S3-T2 are worth mentioning. First, the approximate measurement accuracy and reproducibility for a particular observation is approximately 5%. Thus, a model is not expected to have a prediction accuracy greater than this. Second, the data base consists of data obtained for various times on stream and reaction histories. Some deactivation of the catalyst was observed during the typical time on stream (generally a few hundred hours). Typically, the catalyst would deactivate by 5% before being taken off line. No attempt was made to correct the data for deactivation, nor was there any attempt to account for deactivation in the model. Finally, the rate expression S3-T2, because of its mathematical form, is particularly sensitive to errors in gas composition measurements (fugacities). This can be understood by considering the "driving force" terms in the numerator of the rate expression. Each driving force term consists of a forward and reverse reaction term. For a large fraction of the different reaction conditions in the data base, the methanol synthesis reaction is fairly close to equilibrium. Typically, the difference between the forward and reverse terms is comparable in magnitude to each of the terms. Thus, small gas composition measurement error, particularly with H_2, may cause larger amplitude errors in the rate predictions.

With the above points taken into account, a large fraction of the average absolute prediction error of 12.9% for model S3-T2 can be attributed to the characteristics of the data base. However, it is important to note that some trends, including the effect of feed H_2O addition, are not accurately predicted. This probably means that the model needs improvement and is an oversimplification of reality. Certainly the basic Langmuir-Hinshelwood treatment is intrinsically a simplification. Another possible deficiency of the model is the assumption of water-gas shift equilibrium. Though the S3-85 methanol catalyst is very effective in catalyzing the water-gas shift reaction, the possibility exists that even a small deviation from equilibrium may have a large effect on the methanol rate. In fact, the lack of accuracy in predicting the effect of feed H_2O addition may very well be attributed to this. Further work in model development may yield a better rate expression for methanol synthesis on S3-85.

III. Expansion of the Data Base for S3-86:

In order to expand the S3-86 data base, while also obtaining important data on simulated Great Plains gas, the effect of GHSV on CH_3OH rate was measured for the H_2-rich Great Plains gas matrix with 0.5 mol% and 5 mol% feed CO_2. The intent was to scan as broad a range of GHSV as practical

FIGURE 5

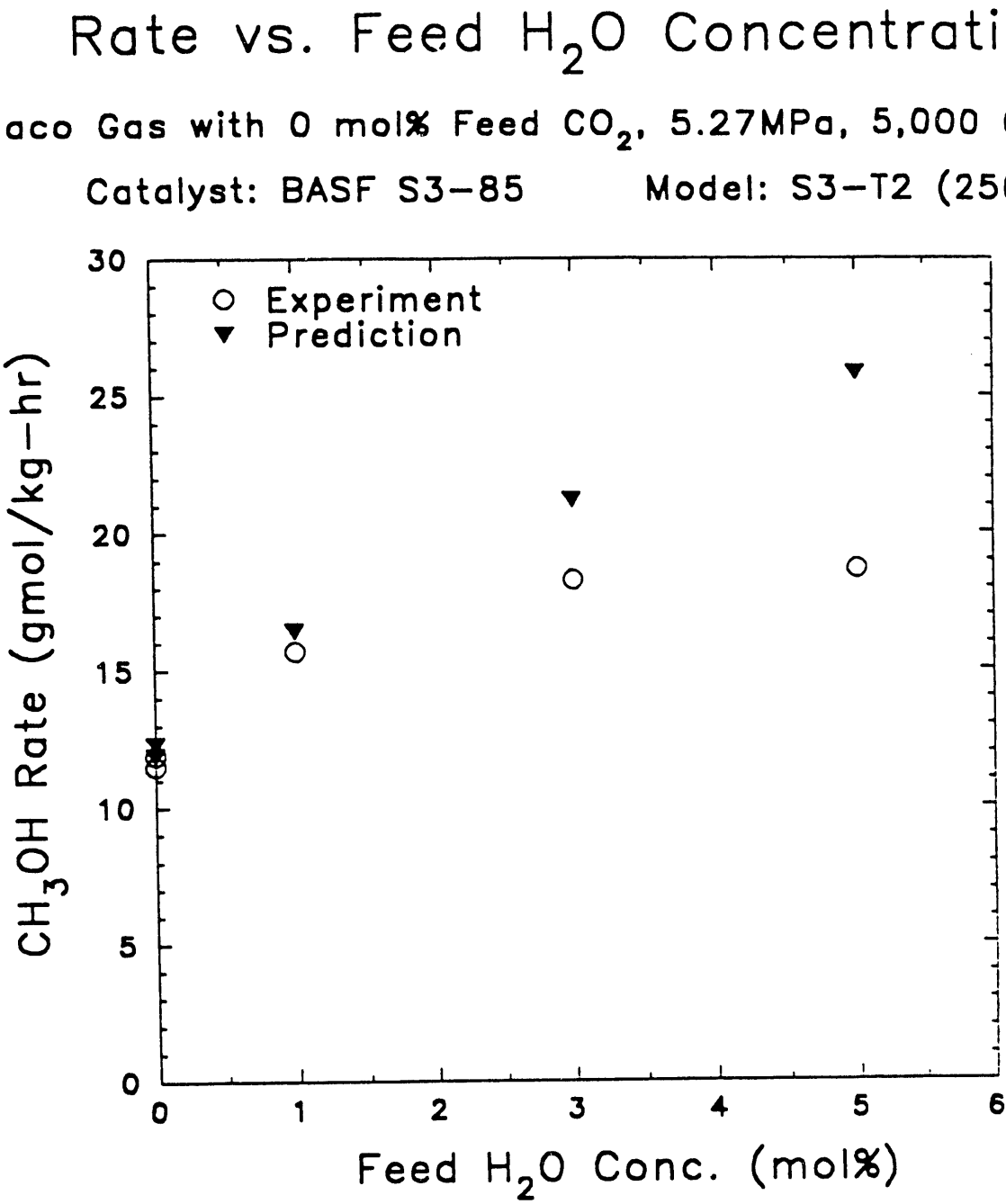
Rate vs. Feed H_2O Concentration
Texaco Gas with 0 mol% Feed CO_2, 5.27MPa, 5,000 GHSV
Catalyst: BASF S3-85
Model: S3-T2 (250°C)
Experiment
Prediction
CH_3OH Rate (gmol/kg-hr)
Feed H_2O Conc. (mol%)
0
5
10
15
20
25
30
0
1
2
3
4
5
6

FIGURE 6

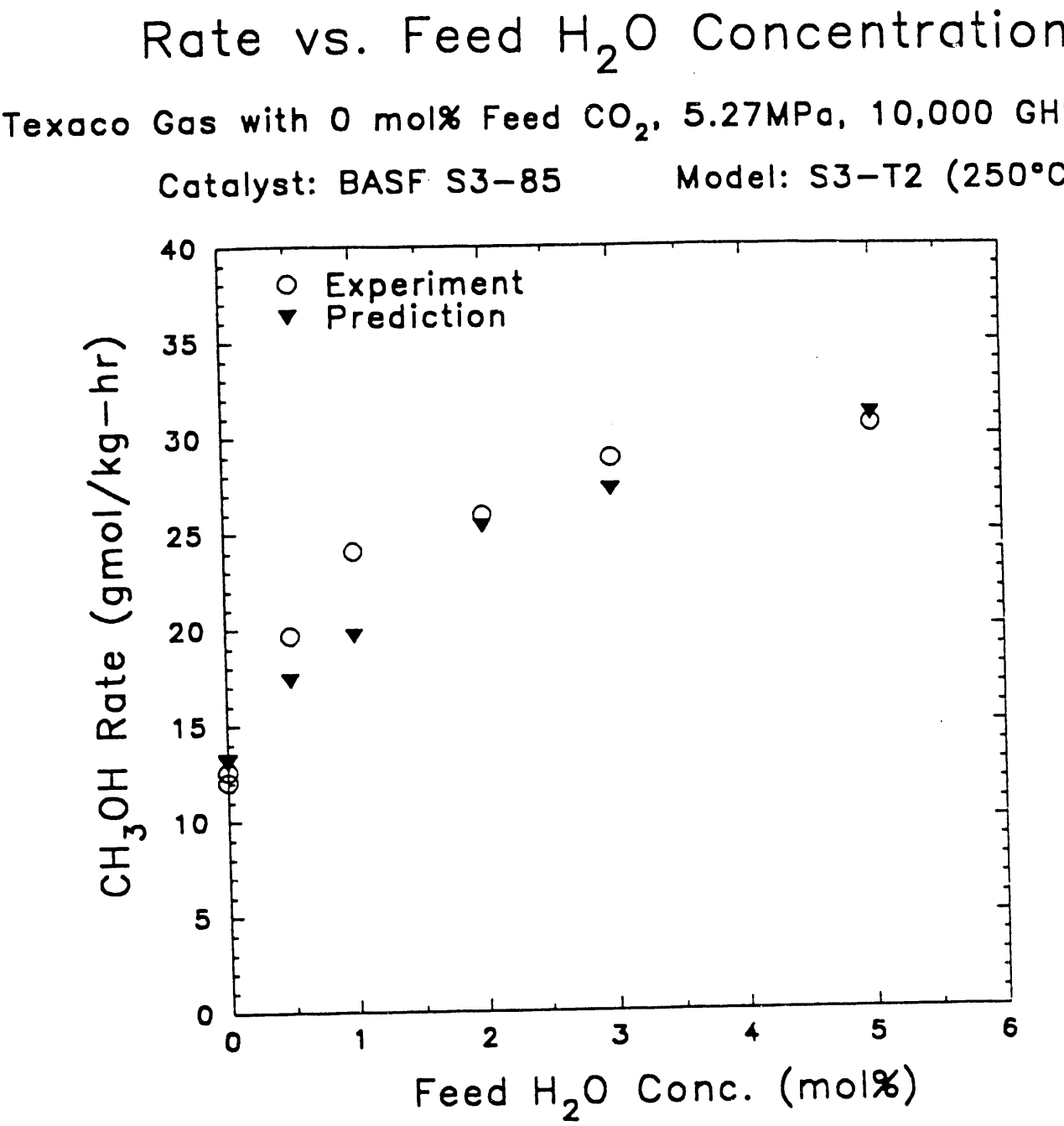
Rate vs. Feed H_2O Concentration
Texaco Gas with 0 mol% Feed CO_2, 5.27MPa, 10,000 GHSV
Catalyst: BASF S3-85
Model: S3-T2 (250°C)
Experiment
Prediction
CH_3OH Rate (gmol/kg-hr)
Feed H_2O Conc. (mol%)
0
5
10
15
20
25
30
35
40
0
1
2
3
4
5
6

FIGURE 7

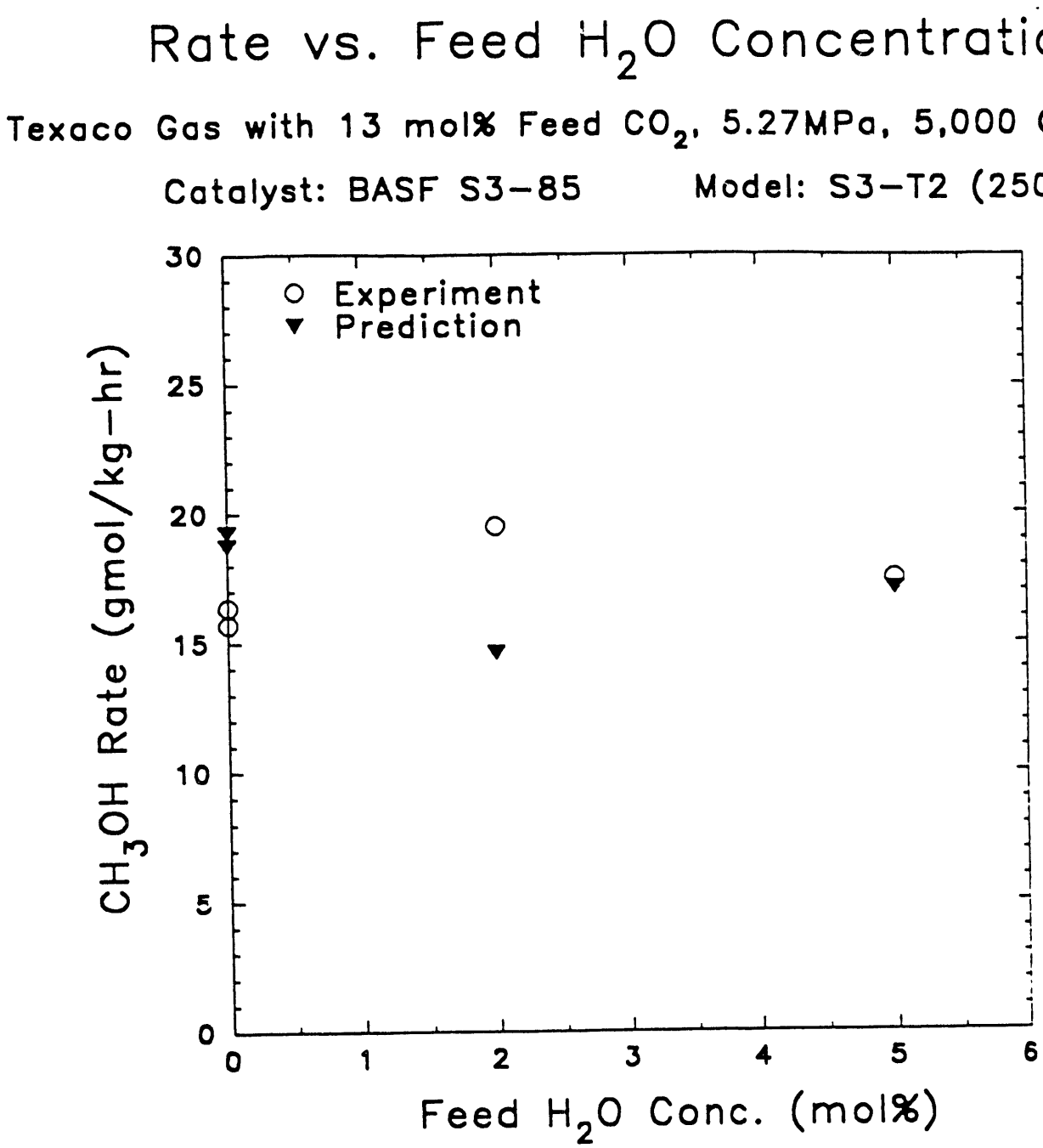
Rate vs. Feed H_2O Concentration
Texaco Gas with 13 mol% Feed CO_2, 5.27MPa, 5,000 GHSV
Catalyst: BASF S3-85
Model: S3-T2 (250°C)
Experiment
Prediction
CH_3OH Rate (gmol/kg-hr)
Feed H_2O Conc. (mol%)
0
5
10
15
20
25
30
0
1
2
3
4
5
6

FIGURE 8

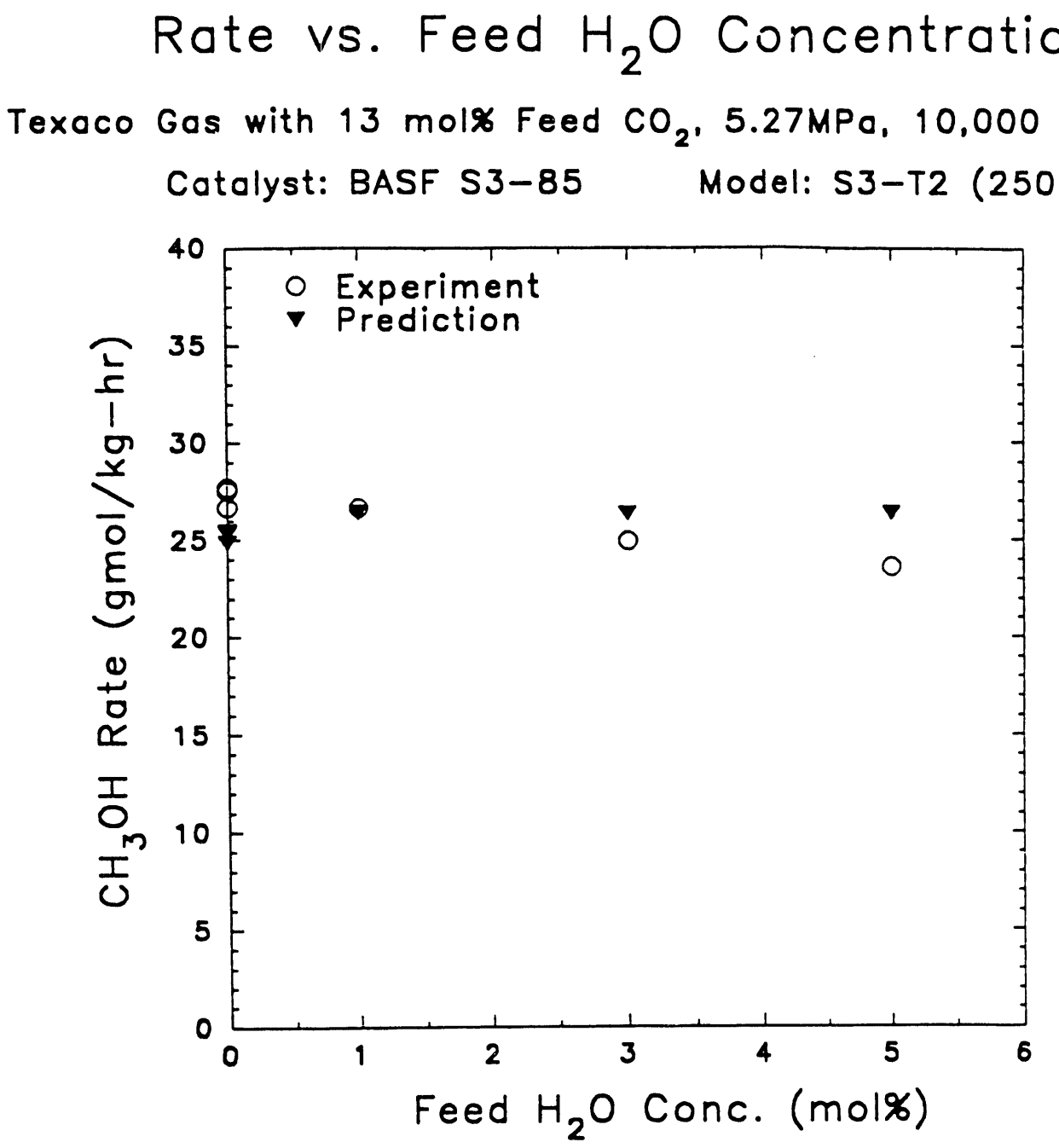
Rate vs. Feed H_2O Concentration
Texaco Gas with 13 mol% Feed CO_2, 5.27MPa, 10,000 GHSV
Catalyst: BASF S3-85
Model: S3-T2 (250°C)
Experiment
Prediction
CH_3OH Rate (gmol/kg-hr)
Feed H_2O Conc. (mol%)
0
5
10
15
20
25
30
35
40
0
1
2
3
4
5
6

FIGURE 9

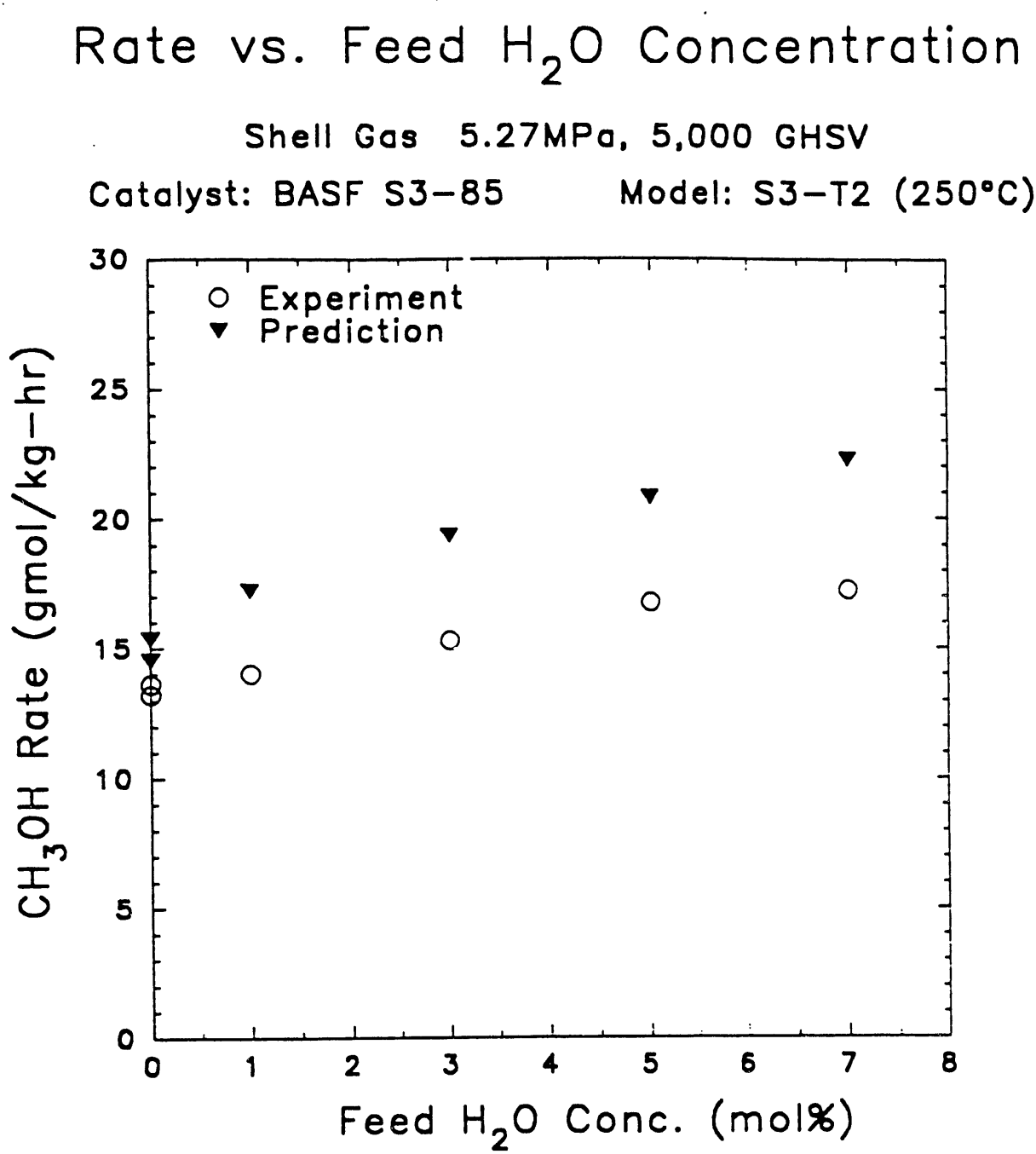
Rate vs. Feed H_2O Concentration
Shell Gas 5.27MPa, 5,000 GHSV
Catalyst: BASF S3-85
Model: S3-T2 (250°C)
Experiment
Prediction
CH_3OH Rate (gmol/kg-hr)
Feed H_2O Conc. (mol%)
0
5
10
15
20
25
30
0
1
2
3
4
5
6
7
8

FIGURE 10

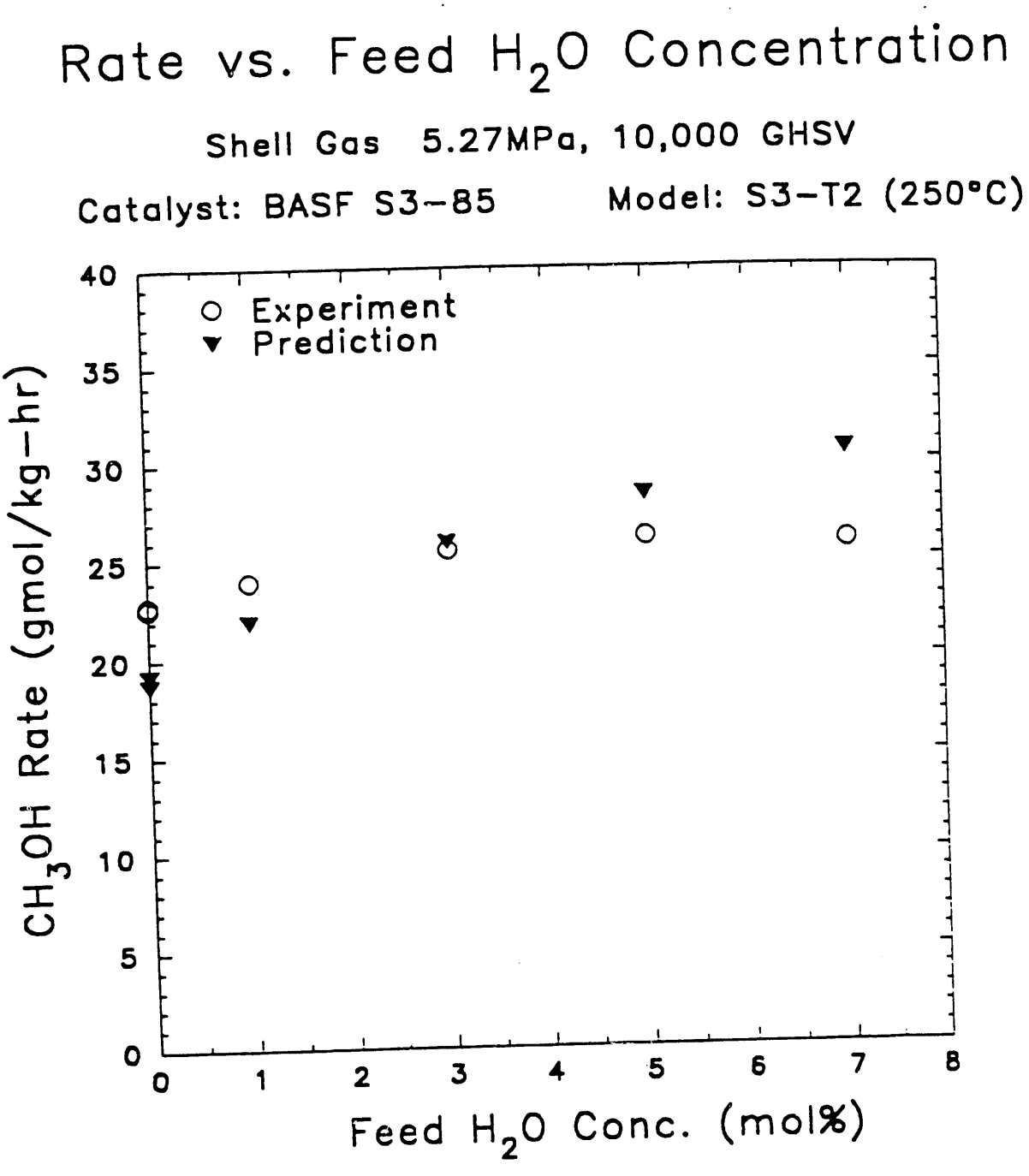
Rate vs. Feed H_2O Concentration
Shell Gas 5.27MPa, 10,000 GHSV
Catalyst: BASF S3-85
Model: S3-T2 (250°C)
Experiment
Prediction
CH_3OH Rate (gmol/kg-hr)
Feed H_2O Conc. (mol%)
0
5
10
15
20
25
30
35
40
0
1
2
3
4
5
6
7
8

in order to provide design data, while at the same time obtaining broad range data that would be a critical test for a reaction model.

Figure 11 shows the effect of GHSV on methanol rate at 5.27 MPa and 250°C for Great Plains gas with 0.5 mol% feed CO_2, that is, no CO_2 addition or removal. The rate was measured at gas-hourly space velocities ranging from 5,000 to 25,000 std. lit./kg-hr. The methanol rate increased from 18 to 38 gmol/kg-hr across this range of GHSV. Comparison with data obtained for Texaco gas at the same conditions indicates that the methanol rate is approximately the same at 5,000 GHSV. However, at higher GHSV, rates observed for Texaco gas are higher. At 10,000 GHSV, the rate for Texaco gas is 32 gmol/kg-hr, while the corresponding rate for Great Plains gas is 25 gmol/kg-hr. Figure 12 shows CH_3OH rate at 5.27 MPa and 250°C as a function of GHSV for Great Plains gas with CO_2 added to the feed at a level of 5 mol%. Comparison with data of Figure 11 for 0.5 mol% feed CO_2 indicates that CO_2 addition dramatically increases the methanol rate across the GHSV range. For example, at 10,000 GHSV, the CH_3OH rate is 62% higher for 5 mol% feed CO_2.

Figure 13 shows the effect of GHSV for the 5 mol% feed CO_2 Great Plains gas at a higher reaction pressure, 7.34 MPa (1050 psig). Comparison with Figure 12 shows that higher reaction pressure increases the CH_3OH rate across the range of GHSV. At 10,000 GHSV, the measured CH_3OH rate at 7.34 MPa is 48.5 gmol/kg-hr compared to 38.2 gmol/kg-hr, an increase of 27%.

The effect of reaction temperature for the 5 mol% CO_2 Great Plains gas at 7.34 MPa was explored using a GHSV of 10,000 std.lit./kg-hr. Figure 14 shows results obtained for 235°C and 255°C, in addition to the 250°C data. The methanol rates measured at 235°C and 255°C are both lower than that observed at 250°C.

The data from Figures 11-13 were entered into the S3-86 data base to be used in the model development. The 235°C and 255°C data points were entered into the data base but were not used in the model development since the data fits were confined to the 250°C data, as mentioned earlier.

IV. Modeling of S3-86 Catalyst Data Base:

Some of the more accurate rate expressions developed for the S3-85 data base were fit to the S3-86 data base. The best-fit parameters were determined using the same technique as that for the S3-85 data base. However, the rate expressions which provided the best fit for the S3-85 data base, yielded poor fits for the S3-86 data base. For example, Models A3-C2 and S3-T2, previously identified in Table 1 in the discussion of the results for S3-85, gave poor fits of the S3-86 data base. The best-fit residual sums of squares for Models A3-C2 and S3-T2 were 7,923 gmol/kg-hr and 6,603 gmol/kg-hr, respectively. Corresponding to these residual sums of squares are average absolute errors per observation of 34.3% for model A3-C2 and 26.3% for model S3-T2. Recall that models A3-C2 and S3-T2 yielded average errors per observation of 13.8% and 12.9%, respectively, for the S3-85 data base. The reason for the poorer fit for the S3-86 data base is probably because the breadth of the S3-86 data base provides a much more discriminating test of the general validity of the model. These rate expressions may provide a good representation of a limited "CO-rich" data base, such as that of S3-85, but are quite deficient for the broader S3-86 data base, which includes extensive data for H_2-rich Great Plains gas.

To find a better model, a variety of other derived rate expressions were investigated for the S3-86 data base. Many of these rate expressions were similar to those investigated for the S3-85 data base.

FIGURE 11

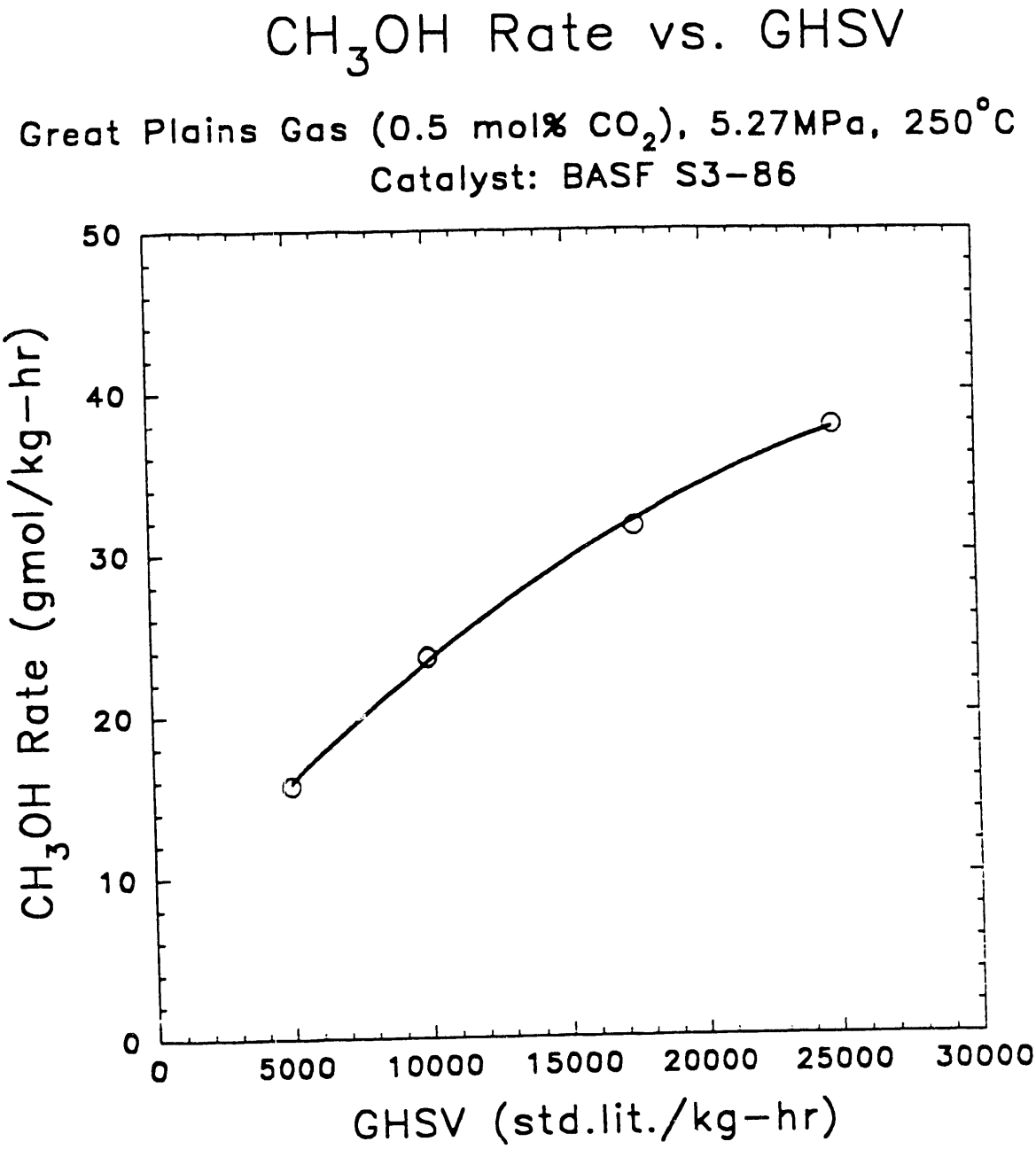
CH3OH Rate vs. GHSV
Great Plains Gas (0.5 mol% CO2), 5.27MPa, 250°C
Catalyst: BASF S3-86
CH3OH Rate (gmol/kg-hr)
50
40
30
20
10
0
0
5000
10000
15000
20000
25000
30000
GHSV (std.lit./kg-hr)

FIGURE 12

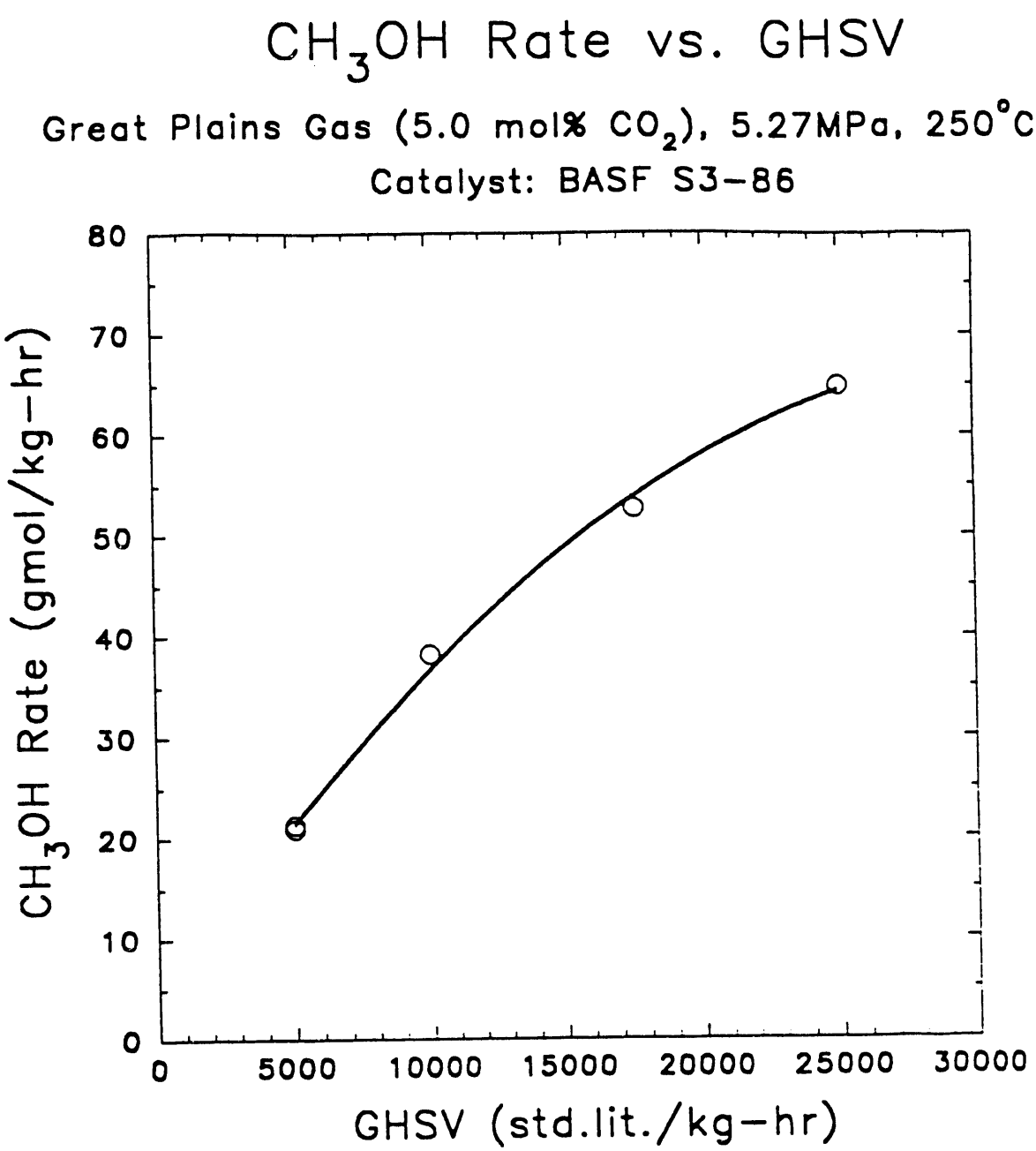
CH3OH Rate vs. GHSV
Great Plains Gas (5.0 mol% CO2), 5.27MPa, 250°C
Catalyst: BASF S3-86
CH3OH Rate (gmol/kg-hr)
GHSV (std.lit./kg-hr)
0
10
20
30
40
50
60
70
80
0
5000
10000
15000
20000
25000
30000

FIGURE 13

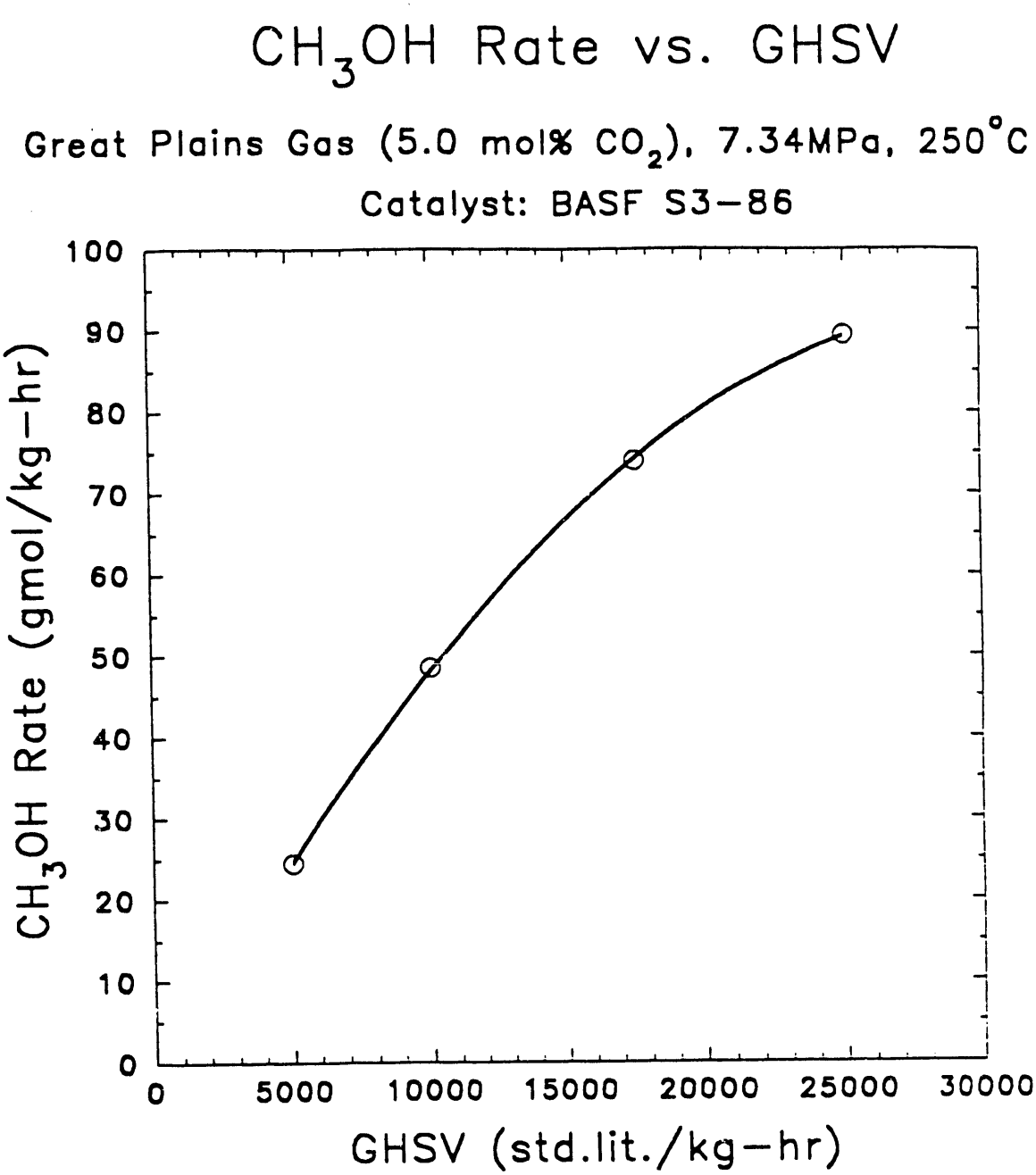
CH3OH Rate vs. GHSV
Great Plains Gas (5.0 mol% CO2), 7.34MPa, 250°C
Catalyst: BASF S3-86
CH3OH Rate (gmol/kg-hr)
100
90
80
70
60
50
40
30
20
10
0
0
5000
10000
15000
20000
25000
30000
GHSV (std.lit./kg-hr)

FIGURE 14

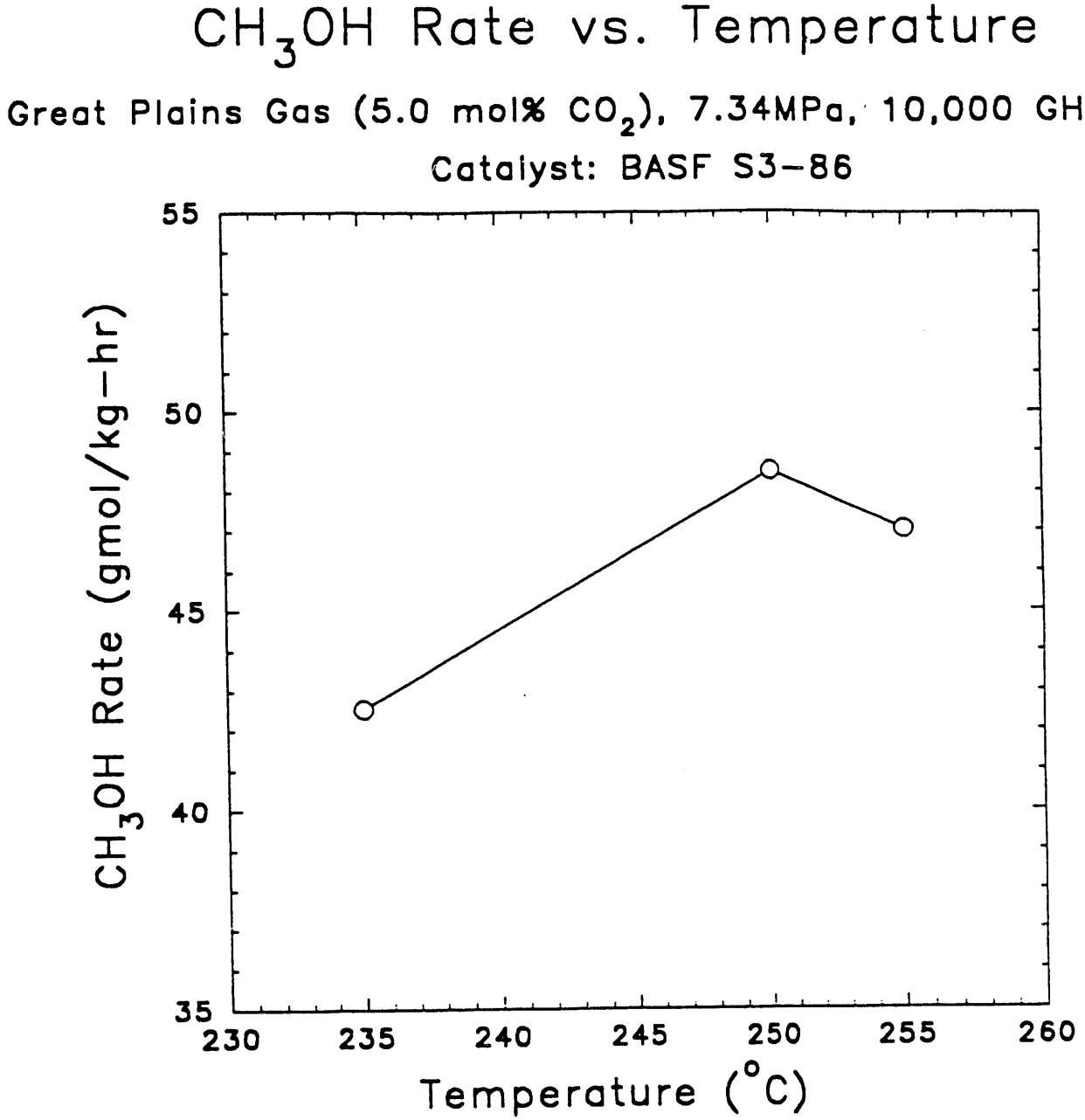
CH3OH Rate vs. Temperature
Great Plains Gas (5.0 mol% CO2), 7.34MPa, 10,000 GHSV
Catalyst: BASF S3-86
CH3OH Rate (gmol/kg-hr)
55
50
45
40
35
230
235
240
245
250
255
260
Temperature (°C)

For example, rate expressions were derived from the mechanism of Graaf et al. [9], like model A3-C2, but with different RDSs and assumptions regarding the dominant adsorbed species. Also, rate expressions derived assuming that CO and CO_2 are stepwise hydrogenated on separate sites (like model S3-T2) were fit to the data, also with a variety of different assumptions regarding the RDSs and adsorption characteristics. Noteworthy is the fact that, in general, rate expressions derived assuming that CO and CO_2 are hydrogenated on separate sites fit the data base better than those derived assuming that CO and CO_2 are hydrogenated on the same site. However, this fact by itself does not provide sufficient evidence that the actual mechanism involves CO and CO_2 hydrogenation on separate sites. The reason for the better fits may be purely a result of the particular mathematical form of the rate expressions.

Another noteworthy reaction mechanism that was considered involves the formation of formate, a species known to exist on operating methanol synthesis catalysts, from the surface reaction of adsorbed CO and -OH. The formate intermediate then undergoes hydrogenation to CH_3OH in a series of steps. The -OH intermediate is either present on the ZnO surface or formed from the hydrogenation of -O from CO_2 dissociation. Langmuir-Hinshelwood rate expressions derived from this mechanism are quite similar in form to those obtained from the above mentioned mechanisms. Rate expressions derived from this mechanism did not fit the data base as well as the best model identified, which is discussed below.

The best model found in this work, designated XX14 and shown in Table 2, was derived from same basic mechanism as that used in the derivation of model S3-T2 for S3-85. Recall that model S3-T2 was derived from a mechanism which assumes that CO and CO_2 are hydrogenated in parallel on separate sites. However, model XX14 has different rate determining steps and different adsorption characteristics than model S3-T2 for S3-85. The different RDSs result in different numerators in the Langmuir-Hinshelwood rate expression, while the different adsorption characteristics result in unique denominators. Specifically, for model XX14, the addition of the first hydrogen atom is the RDS for CO hydrogenation and the addition of the fourth hydrogen atom is the RDS for CO_2 hydrogenation. The adsorption is assumed to be such that the most abundant species on the site that CO is hydrogenated are CH_3OH, H_2O, and vacancies, while the site on which CO_2 is hydrogenated is assumed to be dominated by CH_3OH, CO_2, and vacancies. The result of these assumptions is the six parameter model shown in Table 2. The best-fit residual sum of squares is 2,083, corresponding to an average absolute error per observation of 15.3%.

Also, shown in Table 2 for comparison are the results of fitting the S3-86 data base to rate expressions from the literature. However, note that these rate expressions were cast in terms of fugacities and the assumption of water-gas shift equilibrium was incorporated as required. The parameters in these rate expressions were made adjustable and were determined by the fit. The three rate expressions shown in Table 2 were selected from the literature because they specifically take into account the effect of CO_2. The model designated KL is an adaptation of that of Klier et al. [2], model DJ is due to Dybjaer [12], and model RK is from the recent work of Rinker et al [11]. As can be seen, none of these literature rate expressions fit the S3-86 data base as well as model XX14. Model DJ, from Dybjaer et al, yielded the best fit from these rate expressions, with a residual sum of squares of 4,583 gmol/kg-hr and an average absolute error per observation of 25%.

For model XX14, a compilation of the reactor exit concentrations and calculated fugacities of H_2, CO, CO_2, and CH_3OH, the measured rate, the predicted rate, the residual, and the prediction error is shown in Table B-2 of Appendix B. Figure 15 shows a parity plot, predicted vs. measured CH_3OH

TABLE 2

Rate Expressions for S3-86 Data Base

$K_1 = f_{CH3OH}/f_{CO}(f_{H2})^2 = 0.0018\ atm^{-2}$

Model Name	Rate Expression	Parameter Values	Residual Sum of Squares (gmol/kg-hr)	Avg. Abs Error per Observation (%)
XX14	$r_{CH_3OH} = \dfrac{b_0\left(f_{CO}f_{H_2}^{1/2} - \dfrac{f_{CH_3OH}}{K_1 f_{H_2}^{3/2}}\right)}{\left(1 + b_2 f_{CH_3OH} + b_3\dfrac{f_{CO_2}f_{H_2}}{f_{CO}}\right)^2} + \dfrac{b_1\left(f_{CO_2}f_{H_2}^2 - \dfrac{f_{CH_3OH}f_{CO_2}}{K_1 f_{CO}}\right)}{\left(1 + b_4 f_{CO_2} + b_5 f_{CH_3OH}\right)^2}$	b_0=0.5945 gmol/(kg-hr-atm$^{3/2}$) b_1=0.1603 gmol/(kg-hr-atm^3) b_2=0.0537 atm^{-1} b_3=0.0394 atm^{-1} b_4=0.2242 atm^{-1} b_5=0.1874 atm^{-1}	2,083	15.3
DJ	$r_{CH_3OH} = \dfrac{b_0\left(f_{CO_2}f_{H_2} - \dfrac{f_{CH_3OH}f_{CO_2}}{K_1 f_{CO}f_{H_2}}\right)}{\left(1 + b_1 f_{CO_2}\right)\left(1 + b_2 f_{H_2}^{1/2} + b_3\dfrac{f_{CO_2}f_{H_2}^{1/2}}{f_{CO}}\right)}$	b_0=3.659 gmol/(kg-hr-atm^2) b_1=0.748 atm^{-1} b_2=0 b_3=0.1907 atm$^{-1/2}$	4,583	25.0
KL	$r_{CH_3OH} = \dfrac{b_0\left(\dfrac{f_{CO_2}}{f_{CO}}\right)^3\left(f_{CO}f_{H_2}^2 - \dfrac{f_{CH_3OH}}{K_1}\right)}{\left(1 + b_1\dfrac{f_{CO_2}}{f_{CO}}\right)^3\left(1 + b_2 f_{CO} + b_3 f_{CO_2} + b_4 f_{H_2}\right)^3} + b_5\left(f_{CO_2} - \dfrac{f_{CO_2}f_{CH_3OH}}{K_1 f_{CO}f_{H_2}^2}\right)$	b_0=5852 gmol/(kg-hr-atm^3) b_1=30.96 b_2=0.014 atm^{-1} b_3=0.080 atm^{-1} b_4=0.036 atm^{-1} b_5=0	4,670	22.7
RK	$r_{CH_3OH} = \dfrac{b_0\left(f_{CO}f_{H_2}^2 - \dfrac{f_{CH_3OH}}{K_1}\right)}{\left(f_{CO}f_{H_2}^{3/2} + b_1 f_{H_2} + b_2 f_{CO_2}\right)} + \dfrac{b_3\left(f_{CO_2}f_{H_2} - \dfrac{f_{CH_3OH}f_{CO_2}}{K_1 f_{CO}f_{H_2}}\right)}{\left(f_{CO_2}f_{H_2}^{1/2} + b_4 f_{CO_2}^2 + b_5\left(\dfrac{f_{CO_2}f_{H_2}}{f_{CO}}\right)^3\right)}$	b_0=24.05 gmol/(kg-hr-atm^3) b_1=76.33 atm^{-1} b_2=9.19 atm^{-1} b_3=0 b_4=7.2E+5 atm^{-2} b_5=1.74E+6 atm^{-3}	9,496	31.0

FIGURE 15

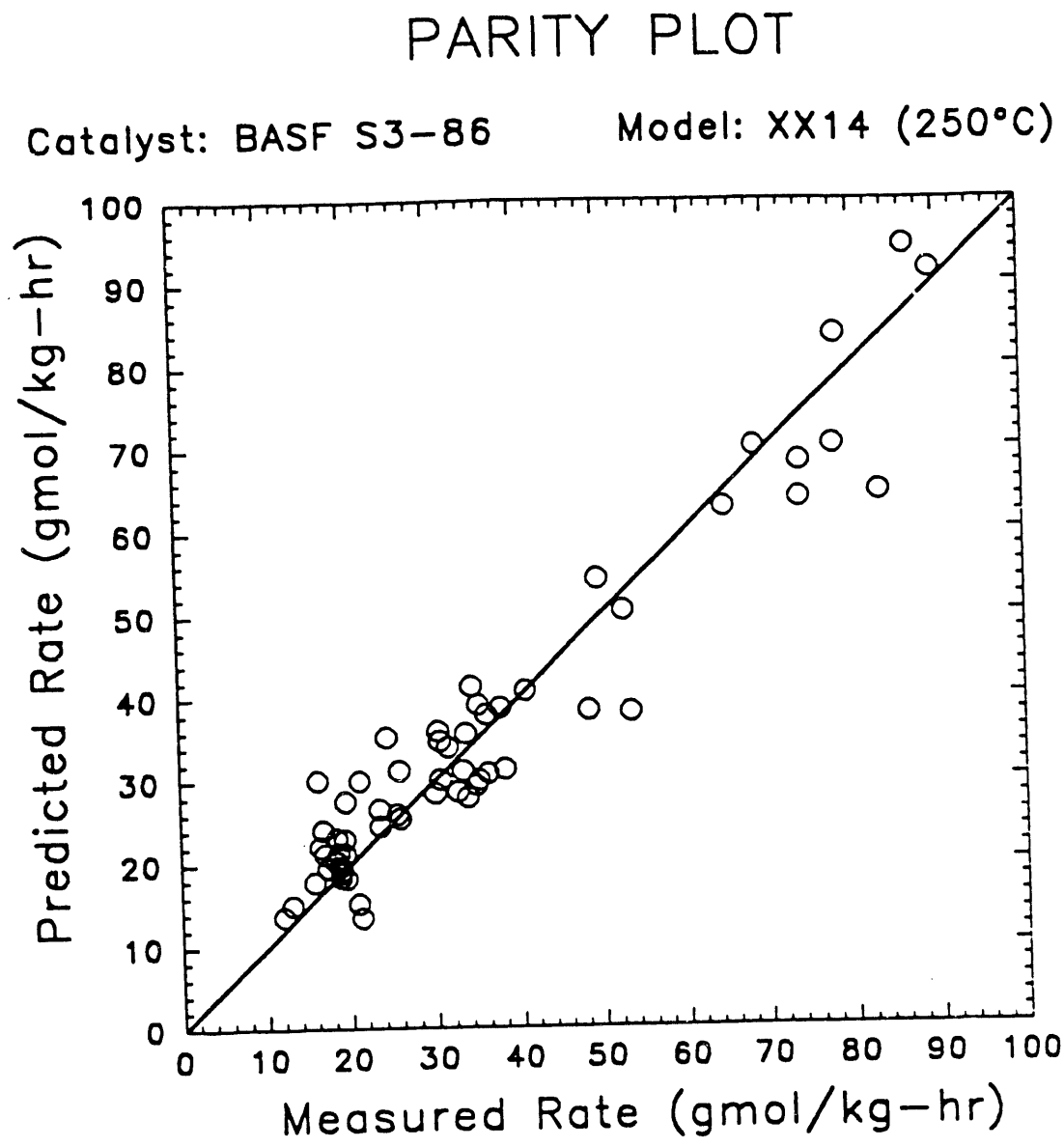
PARITY PLOT
Catalyst: BASF S3-86
Model: XX14 (250°C)
Predicted Rate (gmol/kg-hr)
Measured Rate (gmol/kg-hr)
0
10
20
30
40
50
60
70
80
90
100

rate, for model XX14. The data are fairly evenly scattered about the 45° line. However, there is a slight tendency for the model to overpredict the rate at low measured rates and underpredict the rate at the high measured rates. This results from the fact that the model tends to predict a weaker dependence of the rate on GHSV for the CO-rich gas matrices than that measured. This will be apparent in the discussion below of some of the other comparisons of measured and predicted rate.

Presented next are specific comparisons of measured trends and the corresponding predicted rates. Again, the predicted rates are based on fugacities calculated from the measured reactor exit gas composition and total pressure for each experimental observation.

Figure 16 shows, for model XX14, the measured effect of GHSV on CH3OH rate and the corresponding predicted rates for Texaco gas at 5.27 MPa. The measured effect of GHSV is much steeper than that predicted by the model. Figure 17 shows the measured effect of GHSV and the corresponding predicted rates for Texaco gas at 9.75 MPa. For this pressure, there is good agreement between measured and predicted rate across the range of GHSV. The effect of GHSV on measured rate for Dow gas at 5.27 MPa, along with the model predictions, are shown in Figure 18. The predicted rates at low GHSV are generally slightly higher than the measured rates.

The effect of feed CO_2 concentration on the measured rate for the Great Plains gas matrix at 5.27 MPa, along with corresponding predictions of model XX14, are shown in Figure 19. The measured rate increases dramatically with increasing CO_2 concentration level at the low feed CO_2 concentrations, but levels off at approximately 4-6 mol% feed CO_2. There are some deviations between measured and predicted rate, but the predicted trend is fairly accurate. Figure 20 shows the variation in rate with GHSV, both measured and predicted, for Great Plains gas with 0.5 mol% feed CO_2 at 5.27 MPa. Good agreement between measured and predicted rate exists across the range of GHSV. Figures 21 and 22 show the measured and predicted effect of GHSV for Great Plains gas with 5 mol% feed CO_2 at 5.27 MPa and 7.34 MPa, respectively. Generally good agreement in the trend exists, but there are significant deviations between measured and predicted for some observations. The model tends to underpredict the rate, for all observations, at the lower pressure of 5.27 MPa (Figure 22).

Some additional points regarding model XX14 are worth mentioning. As indicated earlier, the average absolute prediction error per observation for the entire 250°C S3-86 data base was determined to be 15.3%. If the three runs with the highest error are not considered in calculating the average error, the accuracy improves to yield an average absolute error per observation of 13.1%. This is comparable to the accuracy for S3-T2, the model developed for S3-85, which had an average absolute error per observation of 12.9%. This accuracy is quite good considering the effects of experimental error, which were considered in the discussion of the S3-85 results. However, further work would probably yield a more accurate rate expression for the S3-86 data base.

Also, an interesting point to consider is the relative kinetic contribution of CO hydrogenation pathway and the CO_2 hydrogenation pathway to the observed CH_3OH rates. This can be determined by calculating the contribution of each term in the rate expression. Recall that rate expression XX14 is the sum of two terms (see Table 2). From the assumed reaction mechanism, the first term represents the CH_3OH formed from CO hydrogenation, while the second term represents CH_3OH formed from CO_2. The magnitude of each of these terms was determined. For most of the experimental conditions in the data base, these two terms are approximately the same magnitude.

FIGURE 16

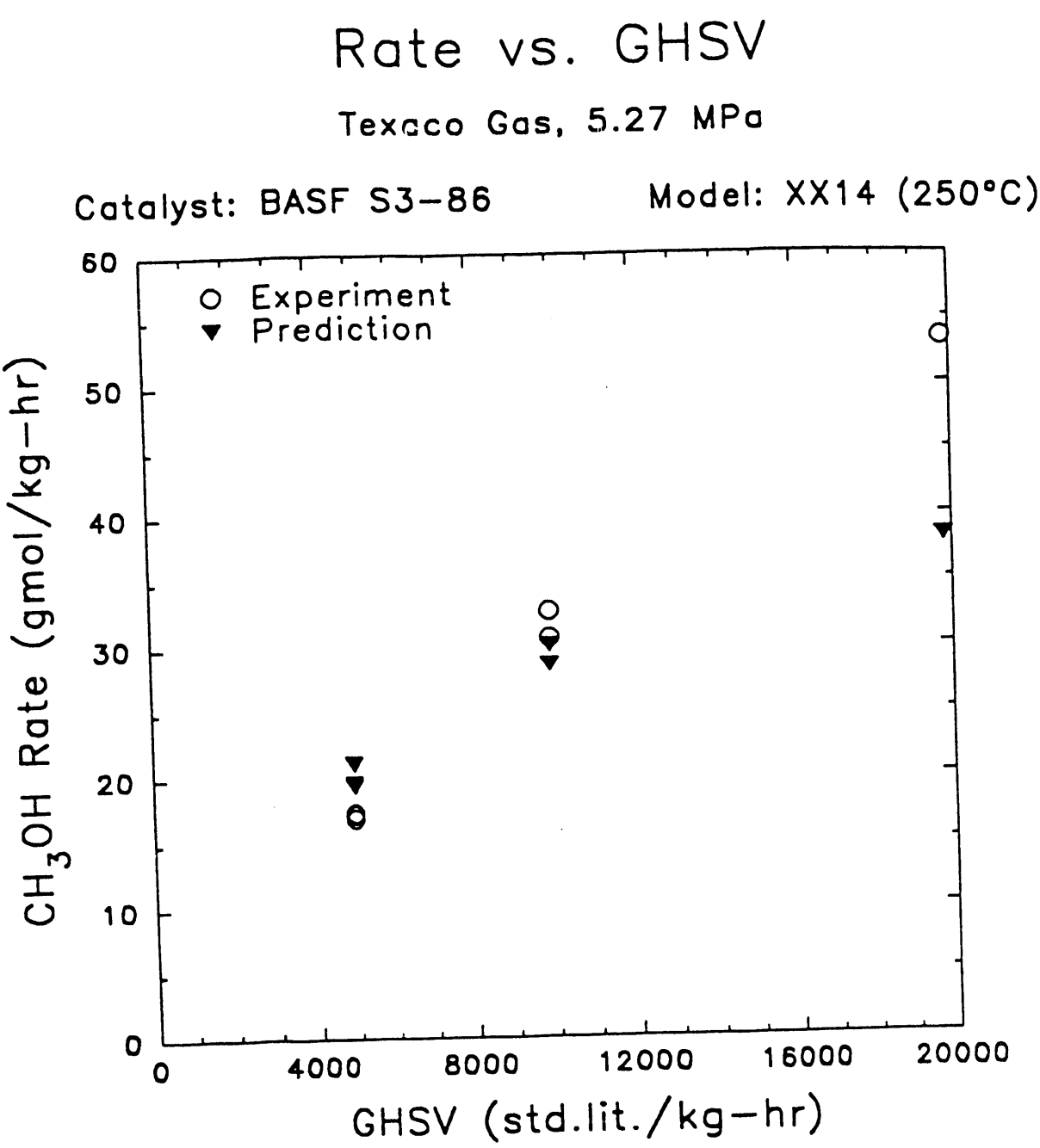
Rate vs. GHSV
Texaco Gas, 5.27 MPa
Catalyst: BASF S3-86
Model: XX14 (250°C)
Experiment
Prediction
CH_3OH Rate (gmol/kg-hr)
GHSV (std.lit./kg-hr)
0
10
20
30
40
50
60
0
4000
8000
12000
16000
20000

FIGURE 17

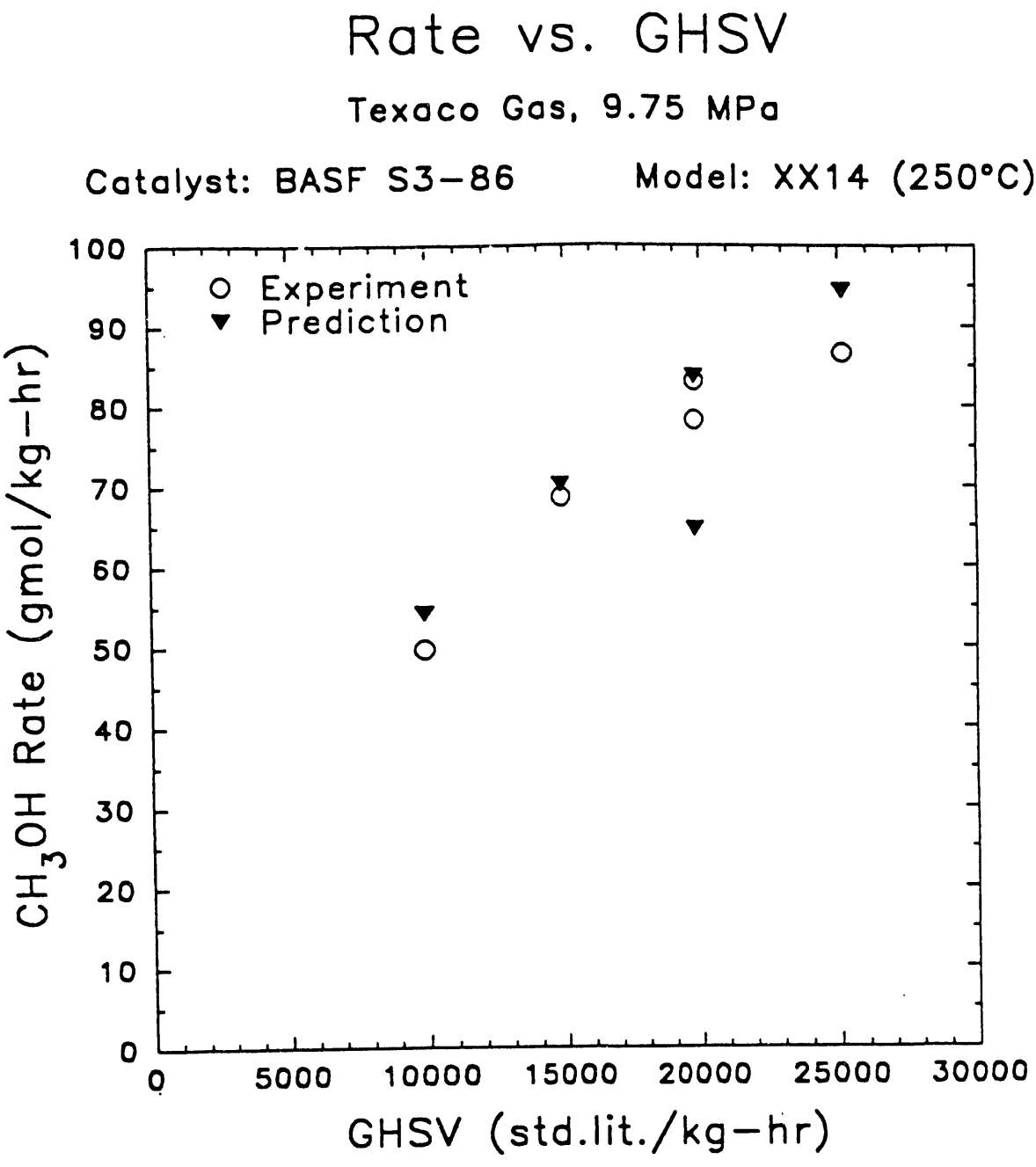
Rate vs. GHSV
Texaco Gas, 9.75 MPa
Catalyst: BASF S3-86
Model: XX14 (250°C)
Experiment
Prediction
CH_3OH Rate (gmol/kg-hr)
GHSV (std.lit./kg-hr)
0
10
20
30
40
50
60
70
80
90
100
0
5000
10000
15000
20000
25000
30000

FIGURE 18

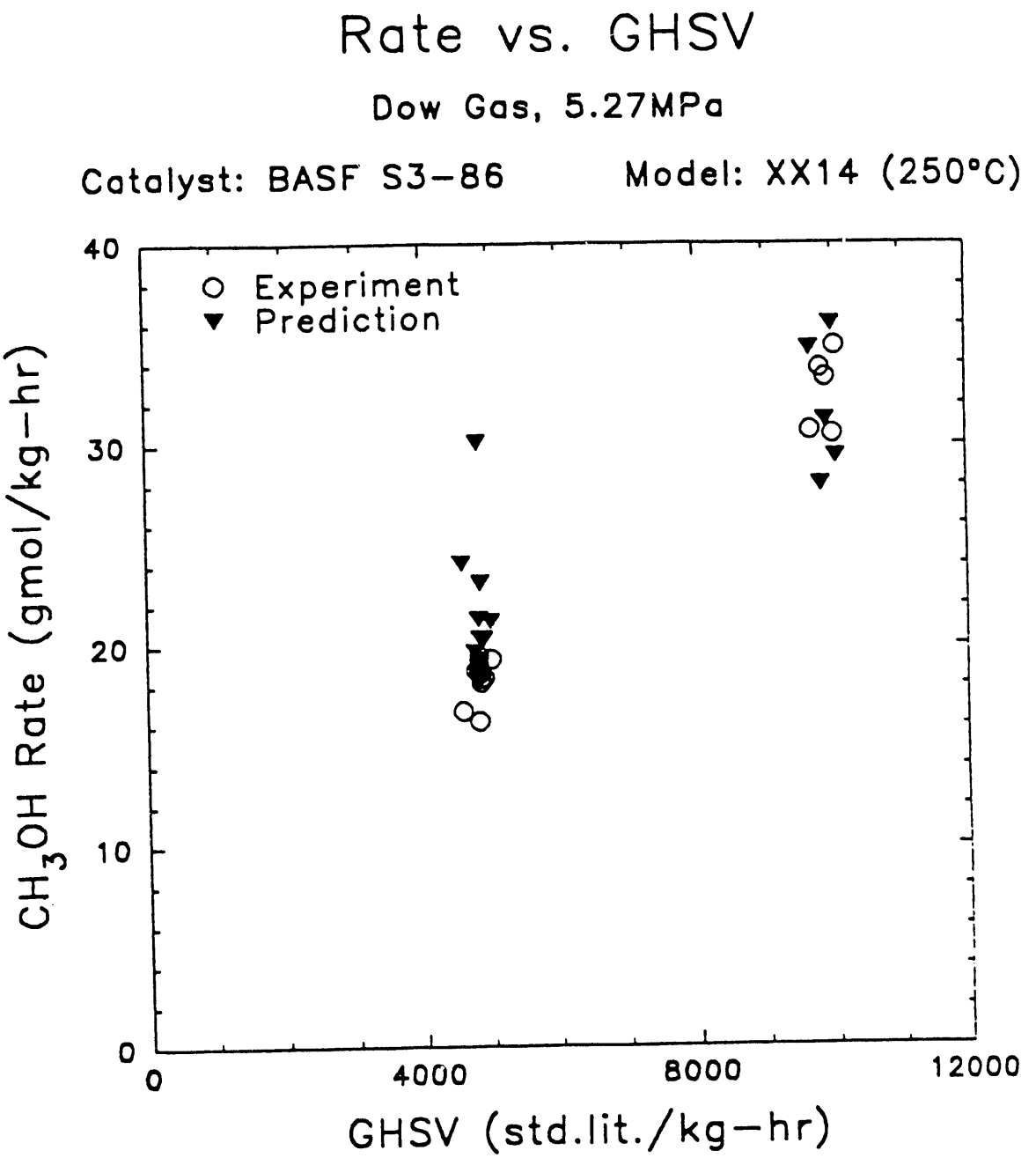
Rate vs. GHSV
Dow Gas, 5.27MPa
Catalyst: BASF S3-86
Model: XX14 (250°C)
Experiment
Prediction
CH_3OH Rate (gmol/kg-hr)
GHSV (std.lit./kg-hr)
0
10
20
30
40
0
4000
8000
12000

FIGURE 19

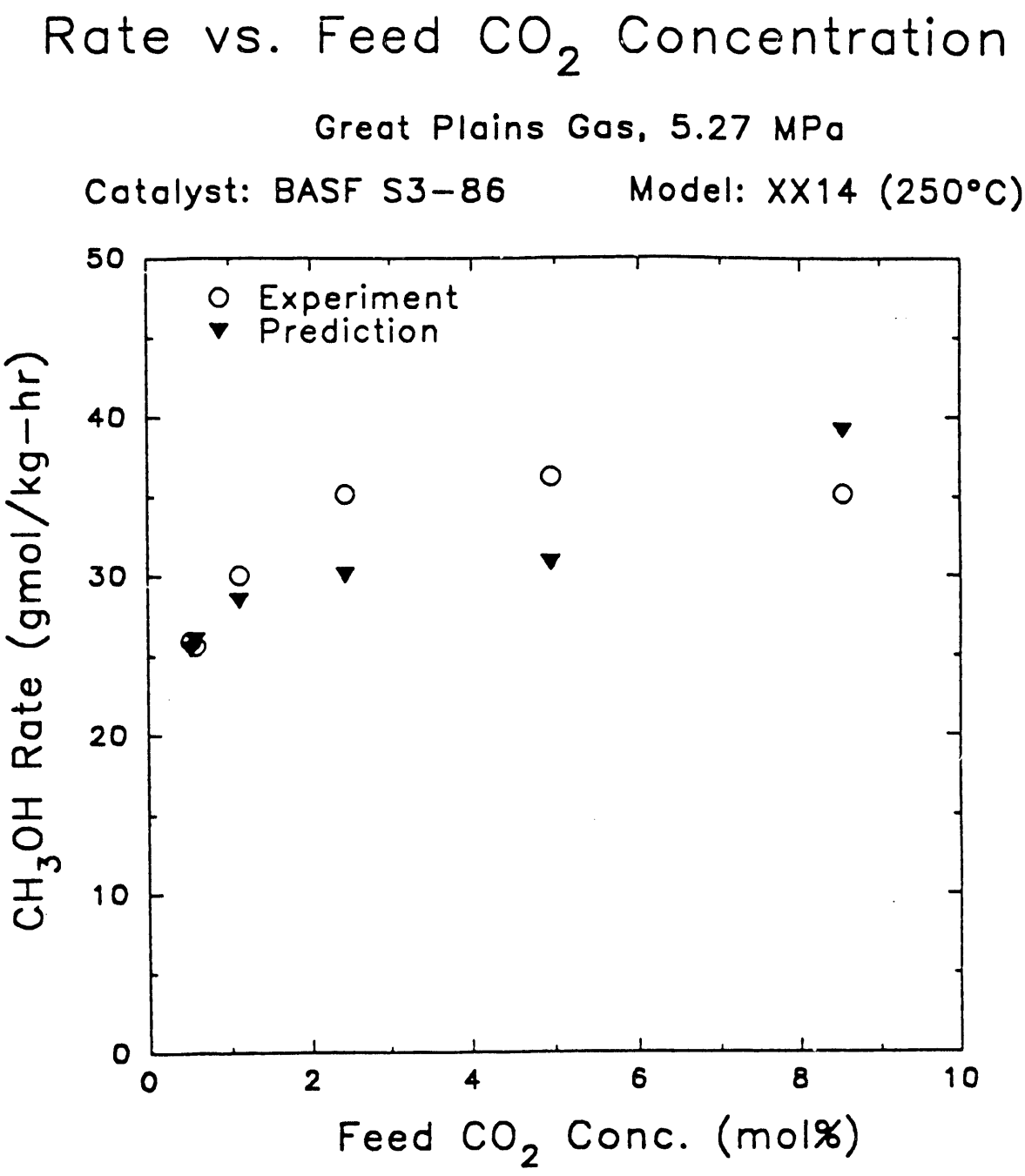
Rate vs. Feed CO_2 Concentration
Great Plains Gas, 5.27 MPa
Catalyst: BASF S3-86
Model: XX14 (250°C)
Experiment
Prediction
CH_3OH Rate (gmol/kg-hr)
Feed CO_2 Conc. (mol%)
0
10
20
30
40
50
0
2
4
6
8
10

FIGURE 20

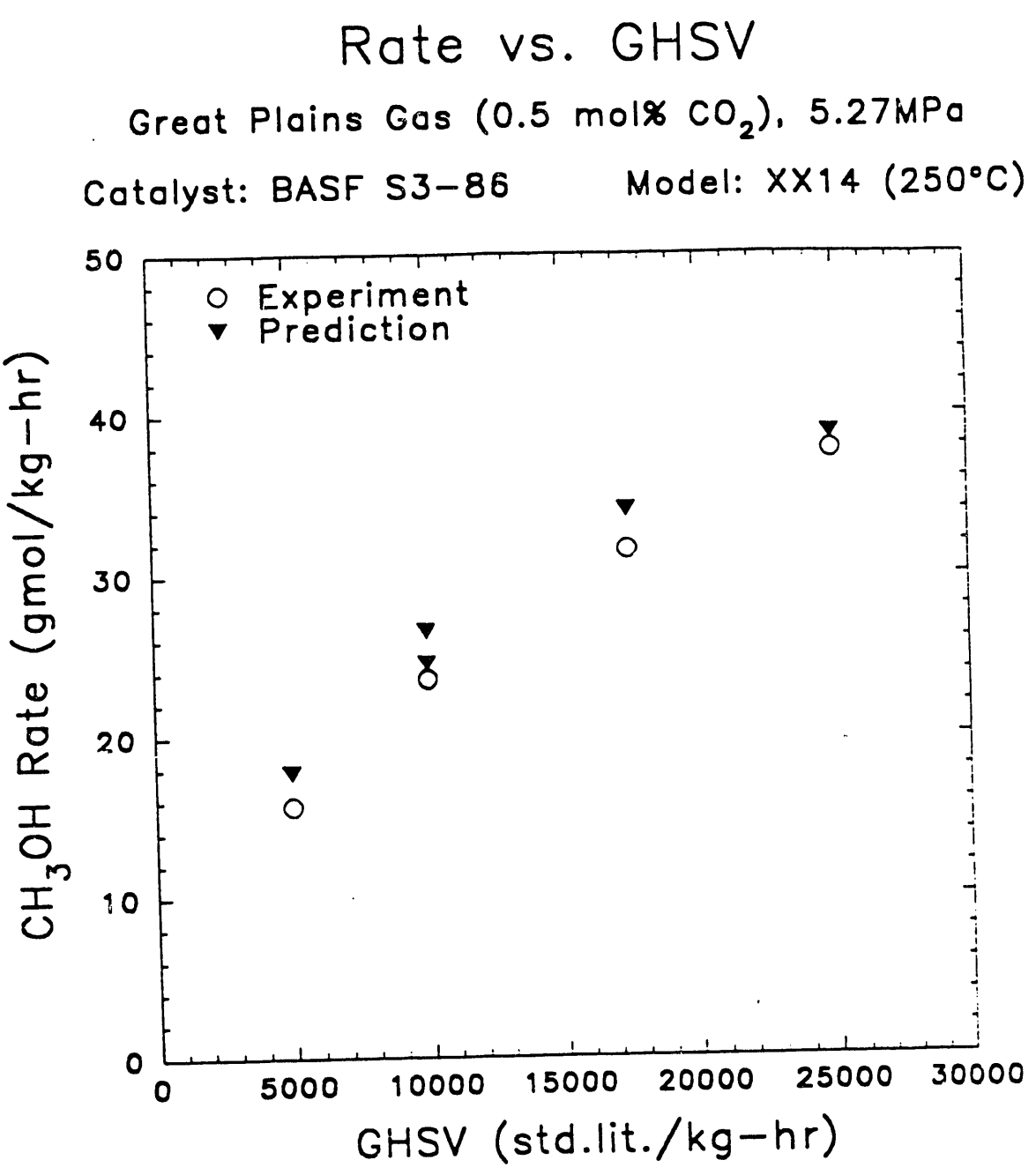
Rate vs. GHSV
Great Plains Gas (0.5 mol% CO_2), 5.27MPa
Catalyst: BASF S3-86
Model: XX14 (250°C)
Experiment
Prediction
CH_3OH Rate (gmol/kg-hr)
GHSV (std.lit./kg-hr)
0
10
20
30
40
50
0
5000
10000
15000
20000
25000
30000

FIGURE 21

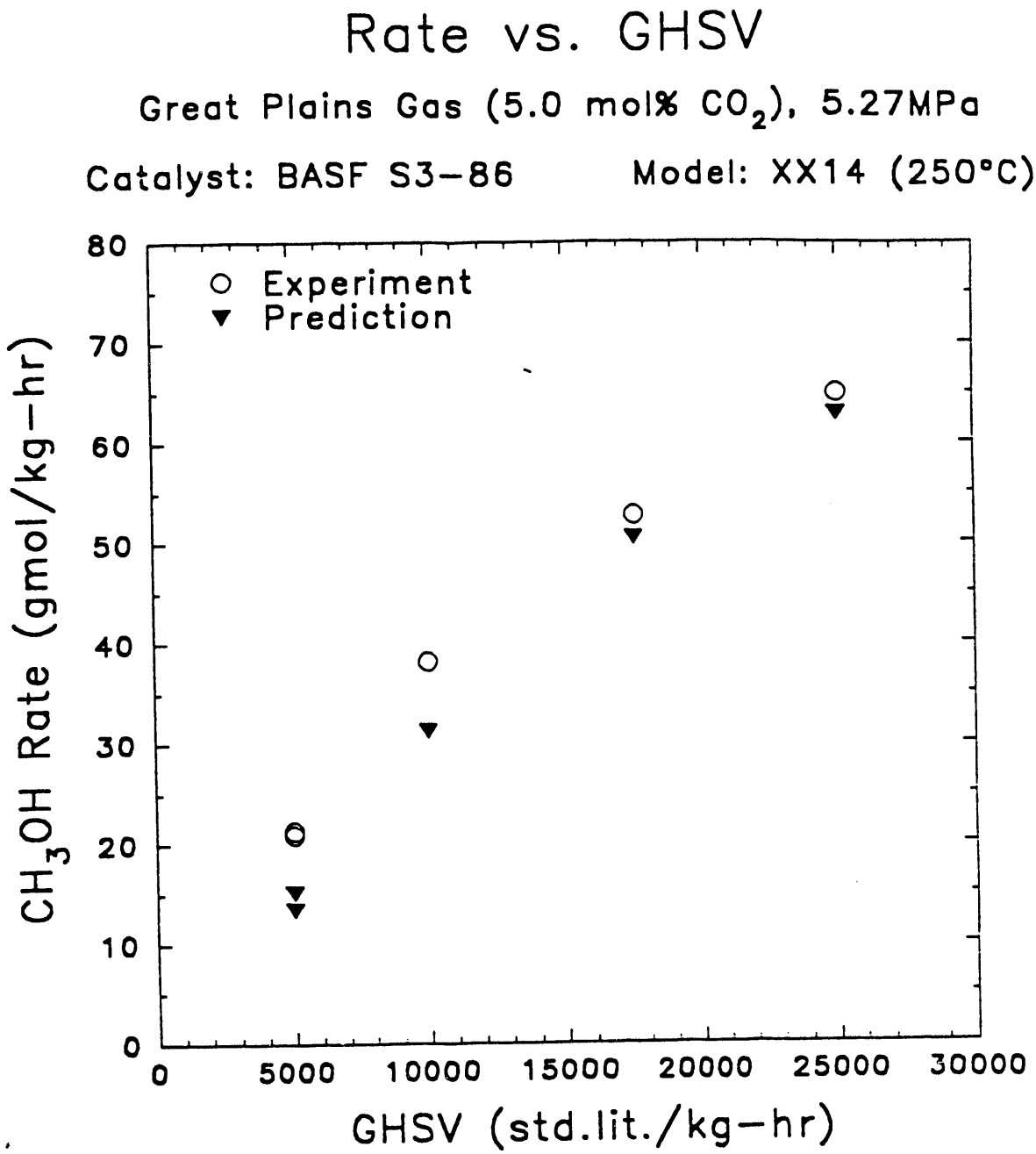
Rate vs. GHSV
Great Plains Gas (5.0 mol% CO_2), 5.27MPa
Catalyst: BASF S3-86
Model: XX14 (250°C)
Experiment
Prediction
CH_3OH Rate (gmol/kg-hr)
GHSV (std.lit./kg-hr)
0
10
20
30
40
50
60
70
80
0
5000
10000
15000
20000
25000
30000

FIGURE 22

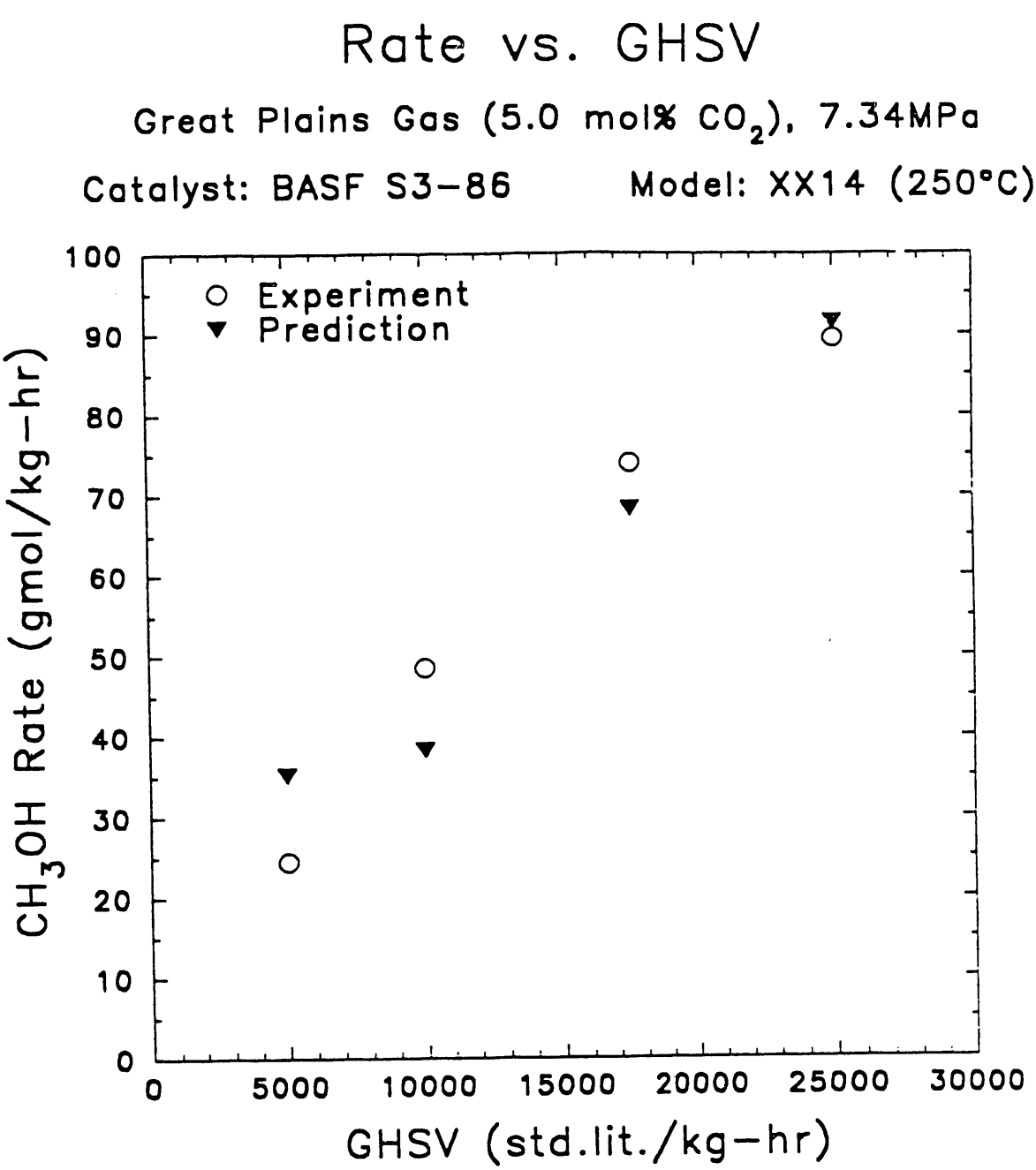
Rate vs. GHSV
Great Plains Gas (5.0 mol% CO_2), 7.34MPa
Catalyst: BASF S3-86
Model: XX14 (250°C)
Experiment
Prediction
CH_3OH Rate (gmol/kg-hr)
GHSV (std.lit./kg-hr)
0
10
20
30
40
50
60
70
80
90
100
0
5000
10000
15000
20000
25000
30000

An exception to this is the runs on Great Plains gas with higher than 0.5 mol% feed CO_2. For these feed conditions, the CO_2 hydrogenation term dominates and is typically an order of magnitude greater than the CO hydrogenation term.

A final point worth mentioning is that the application of model XX14 to the S3-85 data base unfortunately results in a very poor fit. The best fit of that data base yielded a residual sum of squares of 2,708, corresponding to an average error per observation of 21.6%. Furthermore, comparison of measured and predicted rate trends shows very poor agreement in general. The reason why model XX14 does such a poor job in fitting the S3-85 data base is not immediately clear.

SUMMARY AND CONCLUSIONS

Fundamental rate expressions for methanol synthesis were developed to describe the BASF S3-85 and BASF S3-86 methanol catalyst experimental data bases. As part of this work, the BASF S3-86 experimental data base was also expanded with additional experimental measurements on the H_2-rich Great Plains gas matrix. The principal results and conclusions of this work are:

1. Two data bases were constructed comprising all of the laboratory experimental measurements on the S3-85 and S3-86 catalysts. The S3-85 data base is largely concentrated on CO-rich, Texaco feed gas with very limited ranges of pressure and gas-hourly space velocity (GHSV). By contrast, the S3-86 data base includes a much broader range of experimental conditions, including wider ranges of GHSV, pressure, and gas composition. Thus, the S3-86 data base is a more challenging test of a general rate model for methanol synthesis. Neither data base included extensive runs done at temperatures other than 250°C. Therefore, rate expressions were developed for methanol synthesis at 250°C.

2. The data bases for each catalyst were recast in terms of calculated fugacities of H_2, CO, CO_2, and CH_3OH. The fugacity of product H_2O was estimated by assuming water-gas shift equilibrium. The resulting 250°C data base for S3-85 consisted of 112 observations at 69 different conditions, while the 250°C S3-86 data base consisted of 61 observations at 52 different conditions. PC SAS programs were developed to regress the observed methanol rates on the product fugacities and the best-fit models were determined. Procedures were developed to transfer the SAS data to a spreadsheet program where comparisons of predicted and measured rate were generated.

3. A rate expression was developed for the S3-85 data base using an assumed sequence of steps and Langmuir-Hinshelwood kinetics. This rate expression, designated model S3-T2, was derived from a mechanism in which CO and CO_2 are hydrogenated in parallel on separate surface sites by stepwise addition of dissociatively adsorbed hydrogen. The derivation of model S3-T2 assumes that the rate determining steps are the addition of the third hydrogen atom to adsorbed CO and the addition of the second hydrogen atom to adsorbed CO_2. The resulting 4-parameter rate expression is:

$$r_{CH_3OH} = \frac{b_0\left(f_{CO}f_{H_2}^{3/2} - \frac{f_{CH_3OH}}{K_1 f_{H_2}^{1/2}}\right)}{\left(f_{CO} + b_2\frac{f_{CO_2}f_{H_2}}{f_{CO}}\right)^2} + \frac{b_1\left(f_{CO_2}f_{H_2} - \frac{f_{CH_3OH}f_{CO_2}}{K_1 f_{CO}f_{H_2}}\right)}{\left(1 + b_3\frac{f_{CO_2}f_{H_2}}{f_{CO}}\right)^2}$$

This model yields an average absolute error per observation of 12.9%.

4. A rate expression was developed for the S3-86 data base. After screening a variety of mechanisms and combinations of rate-determining steps and adsorption characteristics, a model designated XX14 emerged as the best fit. Like model S3-T2 for S3-85, XX14 was also derived assuming that CO and CO_2 are stepwise hydrogenated on separate surface sites. However, the rate-determining steps and adsorption characteristics are different than those for model S3-T2. The rate determining steps are the addition of the first hydrogen to adsorbed CO and the addition of the fourth hydrogen to adsorbed CO_2. The resulting 6-parameter rate expression is:

$$r_{CH_3OH} = \frac{b_0\left(f_{CO}f_{H_2}^{1/2} - \frac{f_{CH_3OH}}{K_1 f_{H_2}^{3/2}}\right)}{\left(1 + b_2 f_{CH_3OH} + b_3\frac{f_{CO_2}f_{H_2}}{f_{CO}}\right)^2} + \frac{b_1\left(f_{CO_2}f_{H_2}^2 - \frac{f_{CH_3OH}f_{CO_2}}{K_1 f_{CO}}\right)}{\left(1 + b_4 f_{CO_2} + b_5 f_{CH_3OH}\right)^2}$$

This model yields an average absolute error per observation of 15.3%.

5. Three rate expressions obtained from the literature were also fit to the S3-86 data base for purposes of comparison. Model XX14 fit the data much better than any of these literature rate expressions.

6. The parameters in model XX14, the rate expression for S3-86, were made adjustable and the model was fit to the S3-85 data base. The resulting fit was very poor, producing an average absolute error per observation of 21.5%. The reason for the poor fit is not clear.

7. Investigations of various rate models for both data bases indicate that, in general, rate expressions derived from a mechanism in which CO and CO_2 are hydrogenated in parallel on separate sites fit the data better than those derived assuming that CO and CO_2 are hydrogenated on the same site.

8. Because of the mathematical form of rate expressions developed for each catalyst, the prediction accuracy is strongly influenced by the experimental accuracy in measuring reactor exit gas composition. For example, small deviations in the measured H_2 concentration result in much larger deviations in predicted rate. Thus, measurement error contributed significantly to the calculated average prediction error.

9. The S3-86 data base was expanded with experimental runs on the Great Plains gas matrix. The effect of GHSV on the methanol rate was determined for Great Plains gas with 0.5 mol% feed CO_2 at 250°C and 5.27 MPa (750 psig). In addition, methanol rate as a function of GHSV was measured for 5 mol% feed CO_2 at 250°C and pressures of 5.27 MPa and 7.34 MPa. At fixed GHSV and 5.27 MPa, the methanol rate is much greater at the higher feed CO_2 level. At fixed GHSV and 5 mol% feed CO_2, the methanol rate is greater at the higher pressure.

REFERENCES

(1) Herman, R. G., Klier, K., Simmons, G. W., Finn, B. P., Bulko, J. B, and Kobylinski, T. P., J. Catal. 56, 407 (1979).

(2) Klier, K., Chatikavanij, V., Herman, R. G., and Simmons, G. W., J. Catal. 74, 343 (1982).

(3) Rozovskii, A. Ya., Kinet. Katal. 21, 97 (1980).

(4) Kuznetsov, V. D., Shub, F. S., and Temkin, M. I., Kinet. Katal 23, 932 (1982).

(5) Chinchen, G. C., Denny, P. J., Parker, D. G., Spencer, M. S., and Whan, D. A., Appl. Catal. 30, 333 (1987).

(6) Chinchen, G. C., Mansfield, K. and Spencer, M. S., Chemtech, p. 692, November 1990.

(7) Liu, G., Willcox, D., Garland, M., and Kung, H. H., J. Catal. 96, 251 (1985).

(8) Takagawa, M. and Ohsugi, M., J. Catal. 107, 161 (1987).

(9) Graaf, G. H., Stamhuis, E. J., and Beenackers, A. A. C. M., Chem. Eng, Sci. 43, 3185 (1988).

(10) Graaf, G. H., Winkelman, J. G. M., Stamhuis, E. J., and Beenackers, A. A. C. M., Chem. Eng. Sci. 43, 2161 (1988).

(11) McNeil, M. A., Schack, C. J., and Rinker, R. A., Appl. Catal. 50, 265 (1989).

(12) Dybjaer, I., Paper presented at NATO conference on chemical reactor design and technology, 1985. (As referenced in Graaf et al. (9)).

APPENDIX A

TABLE A-1

Syngas Mixtures

	Nominal Composition (mol%)				
Syngas Type	H2	CO	CO2	N2	CH4
Texaco	35	51	13	1	0
Shell	30	66	3	1	0
Dow	44	38	16	2	0
Great Plains	64.5	19	0.5	0	16
"Balanced"	55	19	5	21	0

TABLE A-2

BASF S3-85 Catalyst Data Base

Obs. No.	Run No.	Temp. (C)	Press. (atm)	GHSV (std.lit./kg-hr)	Outlet Gas Composition (mole fraction) H2	CO	CO2	MeOH	N2/CH4	Data Weight Factor	MeOH Rate (gmol/kg-hr)	Syngas Matrix	Special Feed Conditions
1	0270-07	250	52.04	10000	0.2717	0.4966	0.0445	0.0567	---	1.0000	10.71	Texaco	4% feed CO2
2	0067-0	250	52.04	10000	0.2530	0.4969	0.0926	0.0664	---	1.0000	22.73	Texaco	0% feed CO2
3	0269-36	250	52.04	5000	0.2339	0.5235	0.1650	0.0706	---	0.2143	15.66	Texaco	
4	0269-36	250	52.04	5500	0.2593	0.5262	0.1600	0.0642	---	1.0000	24.49	Texaco	
5	7707-30	250	52.04	5000	0.2476	0.5043	0.1576	0.0865	---	1.0000	17.06	Texaco	
6	7707-30	250	52.04	9000	0.2736	0.5015	0.1400	0.0750	---	1.0000	20.69	Texaco	
7	7707-30	250	52.04	14100	0.2010	0.5052	0.1460	0.0624	---	1.0000	35.01	Texaco	
8	0269-14	250	62.24	5000	0.2069	0.5137	0.1674	0.0970	---	0.2143	17.10	Texaco	
9	0447-66	250	52.04	5000	0.4056	0.1330	0.0552	0.0931	---	1.0000	10.43	Balanced	
10	0447-66	250	52.04	10000	0.5160	0.1497	0.0534	0.0695	---	1.0000	27.60	Balanced	
11	0447-66	250	52.04	15000	0.5249	0.1579	0.0522	0.0577	---	1.0000	34.66	Balanced	
12	0447-66	250	52.04	16000	0.5240	0.1567	0.0516	0.0590	---	1.0000	30.14	Balanced	
13	0447-66	250	52.04	10500	0.5242	0.1644	0.0506	0.0484	---	1.0000	36.65	Balanced	
14	0975-102A	249.7	52.02	5000	0.2471	0.5056	0.1525	0.0804	0.0136	0.2143	16.37	Texaco	
15	0975-102B	250.0	52.02	10000	0.2638	0.5012	0.1442	0.0715	0.0129	0.2300	27.73	Texaco	
16	0975-102C	250.0	52.02	5000	0.2510	0.4501	0.1729	0.1019	0.0130	1.0000	19.47	Texaco	2% feed H2O
17	0975-102D	250.4	52.02	5000	0.2402	0.4025	0.1604	0.0030	0.0125	0.2143	15.70	Texaco	
18	0975-102E	250.6	52.02	5000	0.2702	0.4030	0.2076	0.0066	0.0120	1.0000	17.49	Texaco	5% feed H2O
19	0975-102F	251.4	52.02	10000	0.2617	0.4793	0.1474	0.0606	0.0120	0.2300	26.71	Texaco	
20	0975-102G	250.4	52.02	10000	0.2906	0.4313	0.1670	0.0611	0.0116	1.0000	24.91	Texaco	3% feed H2O
21	0975-102H	250.7	52.02	10000	0.2740	0.4697	0.1476	0.0675	0.0122	1.0000	26.61	Texaco	1% feed H2O
22	0975-102I	250.3	52.02	10000	0.3199	0.4045	0.1011	0.0565	0.0114	1.0000	23.61	Texaco	5% feed H2O
23	0975-102J	249.9	52.02	10000	0.3731	0.3643	0.2149	0.0310	0.0106	1.0000	14.35	Texaco	0% feed H2O
24	10111-3C	249.0	52.02	9990	0.2590	0.5044	0.1541	0.0729	0.0109	1.0000	25.96	Texaco	
25	10111-3D	224.0	52.02	9990	0.2904	0.5120	0.1303	0.0465	0.0106	1.0000	10.74	Texaco	
26	10111-3E	225.1	52.02	9990	0.2972	0.4002	0.1552	0.0504	0.0104	1.0000	20.20	Texaco	1% feed H2O
27	10111-3F	224.7	52.02	9990	0.3307	0.4490	0.1763	0.0353	0.0096	1.0000	14.04	Texaco	3% feed H2O
28	10111-3G	250.0	52.02	9990	0.2629	0.5116	0.1426	0.0725	0.0111	0.2300	27.59	Texaco	
29	10111-3H	250.5	52.02	9990	0.2502	0.5011	0.1459	0.0717	0.0109	0.2300	27.56	Texaco	
30	10111-5B	249.2	52.02	5000	0.2311	0.5126	0.1624	0.0936	0.0117	1.0000	16.97	Texaco	
31	10111-5C	249.7	52.02	5000	0.2255	0.4949	0.1821	0.0892	0.0113	0.2143	16.24	Texaco	
32	10111-5D	251.1	52.02	10000	0.2496	0.5032	0.1552	0.0754	0.0111	0.2300	28.10	Texaco	
33	10111-5E	225.0	52.02	10000	0.2019	0.5011	0.1524	0.0515	0.0105	1.0000	20.00	Texaco	
34	10111-5F	225.3	52.02	10000	0.2070	0.4913	0.1590	0.0505	0.0104	1.0000	19.76	Texaco	0.5% feed H2O
35	10111-5G	250.0	52.02	5000	0.2741	0.5421	0.0559	0.1031	0.0147	1.0000	10.99	Texaco	4% feed CO2
36	10111-5H	249.7	52.02	5000	0.2796	0.5577	0.0567	0.1034	0.0152	1.0000	19.07	Texaco	4% feed CO2
37	10111-5I	250.3	52.02	10000	0.3006	0.5520	0.0503	0.0794	0.0141	1.0000	30.77	Texaco	4% feed CO2
38	10111-13B	250.5	52.02	5000	0.2234	0.5099	0.1600	0.0971	0.0097	0.2143	17.30	Texaco	
39	10111-13C	249.2	52.02	5000	0.2205	0.5047	0.1731	0.0974	0.0093	0.2143	17.39	Texaco	
40	10111-13D	250.0	52.02	5000	0.2261	0.4962	0.1647	0.0927	0.0092	0.2143	16.69	Texaco	
41	10111-13E	251.9	52.02	10000	0.2531	0.5015	0.1409	0.0774	0.0092	0.2300	20.75	Texaco	
42	10111-13F	251.1	52.02	5000	0.2517	0.5247	0.1015	0.1069	0.0142	1.0000	19.26	Texaco	0% feed CO2
43	10111-13G	250.5	52.02	10000	0.2769	0.5241	0.0931	0.0854	0.0134	1.0000	32.24	Texaco	0% feed CO2
44	10111-13H	252.5	52.02	10000	0.2021	0.5142	0.1023	0.0863	0.0135	1.0000	32.80	Texaco	0% feed CO2, 1% feed H2O

TABLE A-2

BASF S3-05 Catalyst Data Base

Obs. No.	Run No.	Temp. (C)	Press. (atm)	GHSV (std.lit./kg-hr)	Outlet Gas Composition (mole fraction) H2	CO	CO2	MeOH	N2+CH4	Data Weight Factor	MeOH Rate (gmol/kg-hr)	Syngas Matrix	Special Feed Conditions
45	10111-13I	251.0	52.02	10000	0.3011	0.4001	0.1230	0.0056	0.0131	1.0000	33.37	Tenaco	0% feed CO2, 3% feed H2O
46	10111-13J	250.4	52.02	5000	0.2324	0.5001	0.1560	0.0922	0.0096	0.2143	16.64	Tenaco	
47	10111-13K	250.9	52.02	10000	0.3272	0.4350	0.1461	0.0776	0.0126	1.0000	31.45	Tenaco	0% feed CO2, 5% feed H2O
48	10111-13L	250.1	52.02	10000	0.2024	0.5246	0.0924	0.0026	0.0133	1.0000	31.12	Tenaco	0% feed CO2
49	10111-13M	250.2	52.02	5000	0.2547	0.5255	0.0999	0.1030	0.0141	1.0000	10.03	Tenaco	8% feed CO2
50	10111-13N	250.9	52.02	5000	0.2612	0.5063	0.1111	0.1040	0.0139	1.0000	19.13	Tenaco	8% feed CO2, 1% feed H2O
51	10111-13O	250.0	52.02	5000	0.2794	0.4760	0.1340	0.1079	0.0139	1.0000	20.23	Tenaco	8% feed CO2, 3% feed H2O
52	10111-13P	250.2	52.02	5000	0.2929	0.4294	0.1566	0.1066	0.0132	1.0000	20.47	Tenaco	8% feed CO2, 5% feed H2O
53	10111-13Q	249.1	52.02	10000	0.2294	0.5021	0.1732	0.0921	0.0092	0.2143	16.47	Tenaco	
54	10111-13R	251.2	52.02	5000	0.2993	0.5027	0.1111	0.0002	0.0132	1.0000	31.21	Tenaco	0% feed CO2, 2% feed H2O
55	10111-13S	250.4	52.02	10000	0.2204	0.5172	0.1590	0.0090	0.0096	0.2143	16.24	Tenaco	
56	10111-13T	249.5	52.02	5000	0.3120	0.4705	0.1315	0.0767	0.0130	1.0000	30.74	Tenaco	0% feed CO2, 4% feed H2O
57	10111-13U	249.5	52.02	5000	0.2295	0.5159	0.1517	0.0911	0.0096	0.2143	16.46	Tenaco	
58	10111-13V	249.6	52.02	5303	0.3101	0.6004	0.0056	0.0622	0.0125	1.0000	13.15	Tenaco	0% feed CO2
59	10111-13W	249.5	52.02	5000	0.3070	0.6000	0.0057	0.0640	0.0126	1.0000	11.91	Tenaco	0% feed CO2
60	10111-13X	249.1	52.02	10000	0.3515	0.6063	0.0020	0.0301	0.0121	1.0000	12.06	Tenaco	0% feed CO2
61	10111-13Y	250.2	52.02	10000	0.3179	0.5540	0.0400	0.0757	0.0122	1.0000	20.06	Tenaco	0% feed CO2, 3% feed H2O
62	10111-13Z	250.4	52.02	5000	0.3110	0.6116	0.0048	0.0613	0.0126	1.0000	11.51	Tenaco	0% feed CO2
63	10111-13AA	250.0	52.02	5000	0.2098	0.5570	0.0434	0.1013	0.0129	1.0000	10.27	Tenaco	0% feed CO2, 3% feed H2O
64	10111-13AB	250.0	52.02	5000	0.2900	0.5943	0.0100	0.0071	0.0129	1.0000	15.68	Tenaco	0% feed CO2, 1% feed H2O
65	10111-13AC	250.6	52.02	10000	0.3460	0.6046	0.0022	0.0316	0.0121	1.0000	12.60	Tenaco	0% feed CO2
66	10111-13AD	250.0	52.02	7500	0.3406	0.6060	0.0027	0.0406	0.0122	1.0000	11.05	Tenaco	0% feed CO2
67	10111-13AE	250.5	52.02	2500	0.2710	0.6110	0.0102	0.0923	0.0133	1.0000	7.04	Tenaco	0% feed CO2
68	10111-13AF	250.7	52.02	10000	0.2552	0.5003	0.1575	0.0729	0.0090	0.2300	27.00	Tenaco	
69	10111-13AG	250.9	52.02	10000	0.3210	0.5931	0.0157	0.0633	0.0123	1.0000	24.06	Tenaco	0% feed CO2, 1% feed H2O
70	10111-13AH	250.5	52.02	10000	0.3321	0.5172	0.0652	0.0707	0.0121	1.0000	30.56	Tenaco	0% feed CO2, 5% feed H2O
71	10111-13AI	250.0	52.02	10000	0.2568	0.5119	0.1520	0.0715	0.0091	0.2308	26.70	Tenaco	
72	10111-13AJ	250.4	52.02	3330	0.2709	0.6054	0.0124	0.0059	0.0132	1.0000	9.99	Tenaco	0% feed CO2
73	10111-13AK	249.9	52.02	10000	0.3367	0.5006	0.0006	0.0514	0.0121	1.0000	19.60	Tenaco	0% feed CO2, 0.5% feed H
74	10111-13AL	249.7	52.02	10000	0.3259	0.5610	0.0273	0.0605	0.0121	1.0000	25.91	Tenaco	0% feed CO2, 2% feed H2O
75	10111-13AM	250.5	52.02	5000	0.3130	0.5005	0.0696	0.1021	0.0124	1.0000	18.67	Tenaco	0% feed CO2, 5% feed H2O
76	10111-13AN	249.8	52.02	10000	0.2504	0.5002	0.1532	0.0707	0.0093	0.2300	26.27	Tenaco	
77	10111-13AO	225.4	52.02	5000	0.3506	0.6023	0.0007	0.0252	0.0110	1.0000	5.01	Tenaco	0% feed CO2
78	10111-13AP	226.4	52.02	10000	0.3700	0.6002	0.0005	0.0114	0.0117	1.0000	4.69	Tenaco	0% feed CO2
79	10111-13AQ	250.1	52.02	10000	0.2622	0.5067	0.1530	0.0724	0.0132	1.0000	27.09	Tenaco	
80	10111-13AR	225.5	52.02	10000	0.3560	0.5527	0.0361	0.0405	0.0117	1.0000	16.36	Tenaco	0% feed CO2, 3% feed H2O
81	10111-13AS	225.6	52.02	10000	0.3503	0.5091	0.0124	0.0370	0.0117	1.0000	14.70	Tenaco	0% feed CO2, 1% feed H2O
82	10111-13AT	225.3	52.02	10000	0.3767	0.5365	0.0469	0.0383	0.0116	1.0000	15.82	Tenaco	0% feed CO2, 5% feed H2O
83	10111-22A	249.5	52.02	5000	0.2310	0.4976	0.1615	0.0925	0.0137	0.2143	16.25	Tenaco	
84	10111-22B	249.9	52.02	10000	0.2499	0.5136	0.1573	0.0710	0.0092	0.2300	26.22	Tenaco	
85	10111-22C	250.9	52.02	10000	0.2520	0.5137	0.1576	0.0714	0.0091	0.2300	26.04	Tenaco	
86	10111-22D	250.5	52.02	5000	0.2696	0.5626	0.0552	0.0960	0.0141	1.0000	17.61	Tenaco	4% feed CO2
87	10111-22E	250.4	52.02	10000	0.3024	0.5627	0.0492	0.0744	0.0131	1.0000	20.45	Tenaco	4% feed CO2
88	10111-22F	250.1	52.02	10000	0.3110	0.5430	0.0615	0.0742	0.0129	1.0000	20.69	Tenaco	4% feed CO2, 1% feed H2O

TABLE A-2

BASF S3-85 Catalyst Data Base

Obs. No.	Run No.	Temp. (C)	Press. (atm)	GHSV (std.lit./kg-hr)	Outlet Gas Composition (mole fraction) H2	CO	CO2	MeOH	N2+CH4	Data Weight Factor	MeOH Rate (gmol/kg-hr)	Syngas Matrix	Special Feed Conditions
89	10111-22O	250.3	52.02	10000	0.3255	0.5041	0.0051	0.0753	0.0120	1.0000	29.60	Tenaco	4% feed CO2, 3% feed H2O
90	10111-22H	250.2	52.02	10000	0.3367	0.4011	0.1009	0.0753	0.0125	1.0000	30.26	Tenaco	4% feed CO2, 5% feed H2O
91	10111-22I	250.0	52.02	10000	0.2905	0.5537	0.0402	0.0717	0.0120	1.0000	27.59	Tenaco	4% feed CO2
92	10111-22J	250.4	52.02	5000	0.2754	0.5344	0.0654	0.1002	0.0133	1.0000	18.31	Tenaco	4% feed CO2, 1% feed H2O
93	10111-22K	250.4	52.02	5000	0.2006	0.4903	0.0078	0.1004	0.0130	1.0000	10.69	Tenaco	4% feed CO2, 3% feed H2O
94	10111-22L	250.5	52.02	5000	0.3034	0.4600	0.1120	0.1056	0.0120	1.0000	20.11	Tenaco	4% feed CO2, 5% feed H2O
95	10111-22M	224.7	52.02	5000	0.3009	0.5537	0.0473	0.0740	0.0127	1.0000	14.09	Tenaco	4% feed CO2
96	10111-22N	224.6	52.02	10000	0.3395	0.5502	0.0430	0.0430	0.0121	1.0000	17.79	Tenaco	4% feed CO2
97	10111-22O	250.1	52.02	5000	0.2800	0.5151	0.0773	0.1006	0.0133	1.0000	10.63	Tenaco	4% feed CO2, 2% feed H2O
98	10111-22P	250.5	52.02	5000	0.2938	0.4777	0.0994	0.1013	0.0120	1.0000	19.13	Tenaco	4% feed CO2, 4% feed H2O
99	10111-22Q	250.0	52.02	10000	0.3162	0.5173	0.0704	0.0723	0.0125	1.0000	20.33	Tenaco	4% feed CO2, 2% feed H2O
100	10111-22R	249.9	52.02	10000	0.3250	0.4035	0.0901	0.0733	0.0122	1.0000	29.25	Tenaco	4% feed CO2, 4% feed H2O
101	10111-22S	249.8	52.02	10000	0.2579	0.5077	0.1407	0.0661	0.0008	0.2300	24.45	Tenaco	
102	10111-20A	251.0	52.02	5000	0.2232	0.5055	0.1540	0.0933	0.0103	1.0000	16.40	Tenaco	
103	10111-20B	249.3	52.02	5000	0.2207	0.5009	0.1575	0.0925	0.0095	0.2143	16.28	Tenaco	
104	10111-20C	249.3	52.02	10000	0.2392	0.5002	0.1556	0.0751	0.0009	0.2300	27.24	Tenaco	
105	10111-20D	224.9	52.02	10000	0.3214	0.5449	0.0444	0.0572	0.0122	1.0000	22.64	Tenaco	4% feed CO2
106	10111-20E	236.2	52.02	10000	0.3006	0.5460	0.0467	0.0722	0.0125	1.0000	27.70	Tenaco	4% feed CO2
107	10111-20F	245.4	52.02	10000	0.2930	0.5474	0.0479	0.0701	0.0127	1.0000	29.76	Tenaco	4% feed CO2
108	10111-20G	255.6	52.02	10000	0.2878	0.5481	0.0505	0.0810	0.0130	1.0000	30.03	Tenaco	4% feed CO2
109	10111-20H	249.7	52.02	5000	0.2722	0.5667	0.0297	0.1012	0.0135	1.0000	18.03	Tenaco	2% feed CO2
110	10111-20I	240.2	52.02	10000	0.3066	0.5603	0.0248	0.0697	0.0126	1.0000	26.39	Tenaco	2% feed CO2
111	10111-20J	250.4	52.02	10000	0.3045	0.5675	0.0250	0.0705	0.0125	1.0000	26.64	Tenaco	2% feed CO2
112	10111-20K	250.4	52.02	5000	0.2759	0.5650	0.0293	0.0947	0.0131	1.0000	17.43	Tenaco	2% feed CO2
113	10111-20L	250.5	52.02	10000	0.3004	0.5664	0.0250	0.0705	0.0125	1.0000	26.72	Tenaco	2% feed CO2
114	10111-20M	250.0	52.02	10000	0.2403	0.4535	0.1954	0.0663	0.0119	1.0000	24.06	Tenaco	17% feed CO2
115	10111-20N	249.9	52.02	5000	0.2264	0.4491	0.2031	0.0703	0.0121	1.0000	13.00	Tenaco	17% feed CO2
116	10111-31A	252.5	52.02	5000	0.1907	0.6519	0.0527	0.0717	0.0134	1.0000	13.46	Shell	
117	10111-31B	250.4	52.02	5000	0.2047	0.6652	0.0423	0.0716	0.0133	1.0000	13.63	Shell	
118	10111-31C	249.7	52.02	10000	0.2200	0.6593	0.0372	0.0582	0.0127	1.0000	22.00	Shell	
119	10111-31D	250.3	52.02	10000	0.2300	0.6534	0.0372	0.0573	0.0127	1.0000	22.64	Shell	
120	10111-31E	250.5	52.02	10000	0.2337	0.6373	0.0490	0.0601	0.0127	1.0000	23.97	Shell	1% feed H2O
121	10111-31F	249.8	52.02	10000	0.2450	0.6024	0.0696	0.0629	0.0124	1.0000	25.50	Shell	3% feed H2O
122	10111-31G	249.8	52.02	10000	0.2593	0.5749	0.0840	0.0635	0.0122	1.0000	26.11	Shell	5% feed H2O
123	10111-31H	249.8	52.02	5000	0.2052	0.6550	0.0420	0.0695	0.0130	1.0000	13.22	Shell	
124	10111-31I	249.7	52.02	5000	0.2107	0.6375	0.0535	0.0730	0.0129	1.0000	14.00	Shell	1% feed H2O
125	10111-31J	250.0	52.02	5000	0.2105	0.6026	0.0749	0.0784	0.0129	1.0000	15.29	Shell	3% feed H2O
126	10111-31K	250.5	52.02	5000	0.2341	0.5632	0.0906	0.0846	0.0120	1.0000	16.75	Shell	5% feed H2O
127	10111-31L	250.0	52.02	5000	0.2490	0.5343	0.1155	0.0850	0.0125	1.0000	17.24	Shell	7% feed H2O
128	10111-31M	250.2	52.02	10000	0.2795	0.5263	0.1138	0.0607	0.0117	1.0000	25.07	Shell	7% feed H2O

TABLE A-3

BASF S3-06 Catalyst Data Base

Obs. No	Run No.	Temp. (C)	Press. (atm)	GHSV (std.lit./kg-hr)	Outlet Gas Composition (mole fraction)					Data Height Factor	MeOH Rate (gmol/kg-hr)	Syngas Matrix	Special Feed Conditions
					H2	CO	CO2	MeOH	N2+CH4				
1	10092-31A	250.2	52.02	9901	0.2593	0.4709	0.1522	0.0041	0.0131	1.0000	32.70	Tenaco	
2	10092-31B	250.7	52.02	4951	0.2403	0.4765	0.1571	0.0960	0.0133	1.0000	17.23	Tenaco	
3	10092-31C	250.8	52.02	4951	0.2463	0.4720	0.1506	0.0942	0.0132	1.0000	16.93	Tenaco	
4	10092-31D	249.5	52.02	4951	0.2433	0.4747	0.1501	0.0960	0.0132	1.0000	17.34	Tenaco	
5	10092-31E	249.0	52.02	19002	0.2746	0.4772	0.1520	0.0690	0.0123	1.0000	53.41	Tenaco	
6	10092-31F	250.0	75.03	19002	0.2619	0.4076	0.1200	0.0965	0.0133	1.0000	73.91	Tenaco	
7	10092-31G	250.1	96.24	19002	0.2234	0.4765	0.1590	0.1146	0.0133	1.0000	83.14	Tenaco	
8	10092-31H	250.6	75.03	25149	0.2699	0.4043	0.1431	0.0041	0.0120	1.0000	77.91	Tenaco	
9	10092-31K	250.3	75.03	9901	0.2312	0.4641	0.1507	0.1103	0.0129	1.0000	40.75	Tenaco	
10	10092-31L	225.4	75.03	9901	0.2739	0.4707	0.1444	0.0000	0.0123	1.0000	33.55	Tenaco	
11	10092-31M	225.0	75.03	14052	0.3047	0.4730	0.1359	0.0656	0.0110	1.0000	39.36	Tenaco	
12	10092-31N	224.8	75.03	19002	0.3220	0.4600	0.1359	0.0404	0.0116	1.0000	41.61	Tenaco	
13	10092-31O	225.5	52.02	14052	0.3304	0.4729	0.1396	0.0460	0.0116	1.0000	27.65	Tenaco	
14	10092-31P	224.4	52.02	9901	0.3066	0.4706	0.1461	0.0600	0.0117	1.0000	22.94	Tenaco	
15	10092-31Q	224.9	52.02	4951	0.2663	0.4691	0.1562	0.0907	0.0124	1.0000	10.09	Tenaco	
16	10092-31R	249.7	52.02	9901	0.2632	0.4654	0.1567	0.0011	0.0127	1.0000	30.65	Tenaco	
17	10092-31S	249.4	96.24	19002	0.2501	0.4746	0.1357	0.1042	0.0127	1.0000	78.27	Tenaco	
18	10092-31T	250.0	96.24	25149	0.2641	0.4654	0.1464	0.0900	0.0123	1.0000	86.55	Tenaco	
19	10092-31U	250.5	96.24	14052	0.2334	0.4902	0.1122	0.1260	0.0136	1.0000	60.56	Tenaco	
20	10092-31V	250.1	96.24	9901	0.2123	0.4090	0.1230	0.1421	0.0139	1.0000	49.69	Tenaco	
21	10092-31W	225.2	96.24	9901	0.2565	0.4666	0.1496	0.1197	0.0123	1.0000	45.18	Tenaco	
22	10092-31X	225.0	96.24	14052	0.2082	0.4751	0.1390	0.0033	0.0120	1.0000	50.04	Tenaco	
23	10092-31Y	225.1	96.24	19002	0.3150	0.4675	0.1402	0.0640	0.0115	1.0000	53.72	Tenaco	
24	10092-31Z	225.4	96.24	9901	0.2520	0.4602	0.1596	0.1167	0.0122	1.0000	43.49	Tenaco	
25	9397-93A	240.0	52.02	4573	0.3235	0.3530	0.1909	0.1023	0.0257	1.0000	16.78	Dow	
26	9397-93B	249.9	52.02	4024	0.3340	0.3549	0.1952	0.0919	0.0250	1.0000	16.26	Dow	
27	9397-93C	250.3	52.02	10050	0.3290	0.3575	0.1921	0.0920	0.0246	1.0000	34.07	Dow	
28	9397-93D	249.1	52.02	4024	0.3120	0.3514	0.2016	0.1105	0.0255	1.0000	10.98	Dow	
29	9397-93E	249.9	52.02	4024	0.3116	0.3405	0.2007	0.1136	0.0252	1.0000	19.50	Dow	
30	9397-93F	224.7	52.02	4024	0.3117	0.3530	0.1967	0.1091	0.0250	1.0000	19.00	Dow	
31	9397-93G	225.4	52.02	10000	0.3630	0.3633	0.1797	0.0642	0.0230	1.0000	24.79	Dow	
32	9397-93H	250.4	52.02	9900	0.3330	0.3516	0.1096	0.0902	0.0240	1.0000	33.20	Dow	
33	9397-93I	250.2	52.02	4024	0.3105	0.3470	0.1964	0.1051	0.0245	1.0000	10.58	Dow	
34	9397-93J	239.0	52.02	4024	0.3040	0.3404	0.1990	0.1007	0.0249	1.0000	19.22	Dow	
35	9397-93K	250.0	35.01	5000	0.3577	0.3629	0.1033	0.0669	0.0229	1.0000	12.93	Dow	
36	9397-93L	249.9	62.22	4750	0.2947	0.3500	0.2072	0.1174	0.0255	1.0000	19.46	Dow	
37	9397-93M	249.4	62.22	9000	0.3009	0.3600	0.1924	0.1016	0.0247	1.0000	36.03	Dow	
38	9397-93N	249.7	52.02	5000	0.3100	0.3409	0.1967	0.1055	0.0247	1.0000	19.33	Dow	
39	9397-93O	260.0	52.02	4950	0.3076	0.3327	0.2150	0.0903	0.0249	1.0000	17.34	Dow	
40	9397-93P	260.1	52.02	9000	0.3443	0.3572	0.1075	0.0791	0.0230	1.0000	29.49	Dow	
41	9397-93Q	250.1	52.02	4050	0.3199	0.3504	0.1926	0.1052	0.0247	1.0000	10.30	Dow	
42	9397-93R	250.2	52.02	10000	0.3396	0.3503	0.1070	0.0021	0.0230	1.0000	30.46	Dow	
43	9397-101A	250.3	52.02	4020	0.3020	0.3516	0.1972	0.1004	0.0240	1.0000	10.70	Dow	
44	9397-101B	250.6	52.02	9023	0.3204	0.3502	0.1099	0.0937	0.0241	1.0000	33.76	Dow	

TABLE A-3

BASF S3-06 Catalyst Data Base

Obs. No	Run No.	Temp. (C)	Press. (atm)	GHSV (std.lit./kg-hr)	Outlet Gas Composition (mole fraction)					Data Weight Factor	MeOH Rate (gmol/kg-hr)	Syngas Matrix	Special Feed Conditions
					H2	CO	CO2	MeOH	N2+CH4				
45	9397-101C	250.7	52.02	4046	0.3032	0.3542	0.1977	0.1046	0.0240	1.0000	10.17	Dou	
46	9397-101D	225.2	52.02	4071	0.3046	0.3500	0.1965	0.1110	0.0251	1.0000	19.30	Dou	
47	9397-101F	240.2	52.02	4096	0.2951	0.3544	0.2002	0.1144	0.0225	1.0000	19.66	Dou	
48	9397-1010	249.9	52.02	4096	0.3047	0.3562	0.1901	0.1055	0.0249	1.0000	10.40	Dou	
49	9397-101H	240.1	52.02	5001	0.2966	0.3564	0.1903	0.1127	0.0252	1.0000	20.01	Dou	
50	9397-101I	240.4	52.02	9960	0.3269	0.3632	0.1077	0.0804	0.0239	1.0000	32.31	Dou	
51	9397-101J	239.5	52.02	4020	0.2096	0.3519	0.1997	0.1160	0.0267	1.0000	19.02	Dou	
52	9397-101K	250.6	52.02	4020	0.3031	0.3530	0.1900	0.1104	0.0240	1.0000	10.03	Dou	
53	9397-101L	249.9	35.01	4469	0.3536	0.3629	0.1020	0.0693	0.0230	1.0000	11.90	Dou	
54	9397-101M	239.9	35.01	4670	0.3404	0.3629	0.1044	0.0759	0.0233	1.0000	13.42	Dou	
55	9397-101N	240.6	35.01	9129	0.3609	0.3673	0.1767	0.0560	0.0224	1.0000	20.37	Dou	
56	9397-1010	250.2	52.02	4770	0.3089	0.3476	0.1979	0.1006	0.0249	1.0000	10.76	Dou	
57	9397-101P	250.8	52.02	9675	0.3356	0.3590	0.1073	0.0036	0.0234	1.0000	30.65	Dou	
58	9397-101Q	250.0	62.22	4469	0.2799	0.3497	0.2030	0.1249	0.0256	1.0000	19.37	Dou	
59	9397-101R	250.5	62.22	8032	0.3054	0.3565	0.1930	0.1051	0.0245	1.0000	33.64	Dou	
60	10092-37A	250.4	52.02	9901	0.5351	0.1646	0.0126	0.0606	0.2180	1.0000	25.96	Gr. Plains	1% feed CO2
61	10092-37B	250.4	52.02	4951	0.5409	0.1453	0.0137	0.0905	0.2003	1.0000	16.44	Gr. Plains	1% feed CO2
62	10092-37C	250.2	69.03	9901	0.5325	0.1406	0.0121	0.0924	0.2129	1.0000	34.42	Gr. Plains	1% feed CO2
63	10092-37D	250.3	69.03	4951	0.4925	0.1513	0.0139	0.1139	0.2275	1.0000	21.23	Gr. Plains	5% feed CO2
64	10092-45AT	250.6	52.02	10429	0.5095	0.1302	0.0564	0.0936	0.1994	1.0000	36.21	Gr. Plains	0.5% feed CO2
65	10092-45AU	250.6	52.02	9900	0.5916	0.1464	0.0060	0.0659	0.1861	1.0000	25.63	Gr. Plains	2.5% feed CO2
66	10092-45AV	250.4	52.02	10230	0.5375	0.1395	0.0202	0.0916	0.1942	1.0000	35.14	Gr. Plains	0.5% feed CO2
67	10092-45AW	250.0	52.02	9900	0.5913	0.1451	0.0050	0.0663	0.1841	1.0000	25.90	Gr. Plains	1% feed CO2
68	10092-45AX	250.0	52.02	10100	0.5693	0.1445	0.0121	0.0776	0.1007	1.0000	30.05	Gr. Plains	0.5% feed CO2
69	10092-45AY	250.5	52.02	10770	0.5005	0.1290	0.0934	0.0079	0.1673	1.0000	35.11	Gr. Plains	
70	10092-61A	250.5	52.02	9954	0.5946	0.1544	0.0050	0.0626	0.1796	1.0000	23.54	Gr. Plains	
71	10092-61B	249.5	52.02	9954	0.5602	0.1507	0.0056	0.0665	0.2023	1.0000	23.63	Gr. Plains	
72	10092-61C	250.2	52.02	4977	0.5005	0.1329	0.0060	0.0071	0.1055	1.0000	15.67	Gr. Plains	
73	10092-61D	250.4	52.02	24004	0.6031	0.1731	0.0050	0.0396	0.1792	1.0000	37.76	Gr. Plains	
74	10092-61E	250.6	52.02	17419	0.5966	0.1626	0.0057	0.0495	0.1856	1.0000	31.57	Gr. Plains	
75	0112A27A	250.0	52.02	5000	0.4096	0.1174	0.0598	0.1174	0.1973	1.0000	21.32	Gr. Plains	5% feed CO2
76	0115A05A	250.0	52.02	10000	0.5255	0.1327	0.0505	0.0973	0.1957	1.0000	30.22	Gr. Plains	5% feed CO2
77	0115A16A	250.0	52.02	5000	0.5006	0.1176	0.0609	0.1170	0.2011	1.0000	20.91	Gr. Plains	5% feed CO2
78	0115A21A	250.0	52.02	25002	0.5303	0.1526	0.0531	0.0633	0.1020	1.0000	64.02	Gr. Plains	5% feed CO2
79	0116A02A	250.0	52.02	17499	0.5465	0.1458	0.0546	0.0760	0.1896	1.0000	52.69	Gr. Plains	5% feed CO2
80	0116A13A	250.0	72.43	10000	0.4836	0.1060	0.0608	0.1367	0.2041	1.0000	40.51	Gr. Plains	5% feed CO2
81	0117A00A	250.0	72.43	25002	0.5411	0.1371	0.0530	0.0900	0.1933	1.0000	09.47	Gr. Plains	5% feed CO2
82	0117A13A	250.0	72.43	17499	0.5192	0.1249	0.0570	0.1093	0.1964	1.0000	74.00	Gr. Plains	5% feed CO2
83	0117A22A	250.0	72.43	5000	0.4070	0.1007	0.0641	0.1406	0.2065	1.0000	24.53	Gr. Plains	5% feed CO2
84	0118A12A	235.0	72.43	10000	0.5106	0.1184	0.0509	0.1158	0.1973	1.0000	42.55	Gr. Plains	5% feed CO2
85	0118A22A	255.0	72.43	10000	0.5049	0.1104	0.0592	0.1305	0.2000	1.0000	47.04	Gr. Plains	5% feed CO2

APPE. IDIX B

TABLE B-1

Model S3-T2 Fit to all 250 C data (S385 250)

Residual Sum of Squares = 1029.57
Average Absolute Error per Observation = 12.87 %

B0 = 4.7313 B2 = 0.446
B1 = 1.2201 B3 = 0.2676

Obs. #	YH2	YCO	YCO2	YCH3OH	MEAS. RATE	DATA WT	FH2	FCO	FCO2	FCH3OH	PRED RATE	RESID.	% ERROR
49	0.2547	0.5255	0.0999	0.1030	10.03	1	13.7905	27.0307	5.1136	4.0743	10.07	-0.04	-0.21
50	0.2612	0.5063	0.1111	0.1040	19.13	1	14.1546	26.8267	5.691	4.9263	19.03	0.10	0.51
51	0.2794	0.4768	0.134	0.1079	20.23	1	14.9245	24.8916	6.7574	4.9939	18.93	1.30	6.42
52	0.2929	0.4294	0.1566	0.1066	20.47	1	15.8505	22.7067	7.9955	4.9991	18.26	2.21	10.80
53	0.2294	0.5021	0.1732	0.0921	16.47	0.2143	12.3443	26.3793	8.7706	4.2656	15.13	1.34	8.14
54	0.2993	0.5027	0.1111	0.0802	31.21	1	16.0014	26.3897	5.6494	3.7767	27.78	3.43	10.98
55	0.2284	0.5172	0.1598	0.0890	16.24	0.2143	12.2975	27.2065	8.1099	4.1772	16.45	-0.21	-1.29
56	0.3128	0.4705	0.1315	0.0767	30.74	1	16.7504	24.7407	6.7002	3.6154	27.83	2.91	9.48
57	0.2295	0.5159	0.1517	0.0911	16.46	0.2143	12.4432	27.3261	7.751	4.2656	16.70	-0.24	-1.47
58	0.3101	0.6084	0.0056	0.0622	13.15	1	16.6412	32.2212	0.2061	2.9912	12.46	0.69	5.27
59	0.307	0.608	0.0057	0.064	11.91	1	16.5059	32.2472	0.2965	3.0796	12.33	-0.42	-3.56
60	0.3515	0.6063	0.002	0.0301	12.06	1	18.7324	32.0443	0.104	1.4618	13.22	-1.16	-9.66
61	0.3179	0.554	0.04	0.0757	28.86	1	17.0678	29.2977	2.0548	3.6154	27.18	1.68	5.83
62	0.3118	0.6116	0.0048	0.0613	11.51	1	16.6724	32.2888	0.2445	2.9391	11.94	-0.43	-3.76
63	0.2898	0.5578	0.0434	0.1013	18.27	1	15.5332	29.3341	2.2109	4.765	21.19	-2.92	-15.97
64	0.2900	0.5943	0.0180	0.0071	15.60	1	15.5748	31.3004	0.9624	4.1252	16.44	-0.76	-4.84
65	0.346	0.6046	0.0022	0.0316	12.6	1	18.5399	32.1276	0.1144	1.545	13.13	-0.53	-4.20
66	0.3406	0.6068	0.0027	0.0406	11.05	1	18.1490	32.0287	0.1405	1.9664	12.09	-1.04	-0.79
67	0.2718	0.6118	0.0102	0.0923	7.84	1	14.6384	32.372	0.5254	4.3801	10.67	-2.83	-36.12
68	0.2552	0.5083	0.1575	0.0729	27.00	0.2308	13.7229	26.7799	8.0215	3.4229	23.89	3.19	11.79
69	0.3218	0.5931	0.0157	0.0633	24.06	1	17.1406	31.1808	0.8011	3.0224	19.64	4.42	18.37
70	0.3321	0.5172	0.0652	0.0787	30.56	1	17.7388	27.1909	3.3293	3.735	31.02	-0.46	-1.51
71	0.2568	0.5119	0.152	0.0715	26.78	0.2308	13.8269	27.0088	7.7562	3.3657	24.69	2.09	7.79
72	0.2709	0.6054	0.0124	0.0859	9.99	1	15.0598	32.1484	0.6398	4.0992	12.80	-2.81	-28.14
73	0.3367	0.5086	0.0086	0.0514	19.60	1	18.0613	31.2276	0.4422	2.4918	17.36	2.32	11.81
74	0.3259	0.561	0.0273	0.0605	25.91	1	17.5672	29.8231	1.4097	3.3033	25.32	0.59	2.26
75	0.313	0.5005	0.0696	0.1021	18.67	1	16.9013	26.5094	3.5738	4.8379	25.78	-7.11	-38.09
76	0.2504	0.5082	0.1532	0.0707	26.27	0.2308	13.6136	27.0712	7.8914	3.3553	24.25	2.02	7.69
79	0.2622	0.5067	0.153	0.0724	27.09	1	14.0298	26.5718	7.7562	3.3865	24.61	2.48	9.15
83	0.231	0.4976	0.1615	0.0925	16.25	0.2143	12.5472	26.3949	8.2600	4.3333	15.62	0.63	3.89
84	0.2499	0.5136	0.1573	0.0718	26.22	0.2308	13.4576	27.0068	8.0163	3.3709	23.78	2.44	9.31
85	0.2520	0.5137	0.1576	0.0714	26.04	0.2300	13.5660	27.0192	8.0163	3.3501	24.07	1.97	7.55
86	0.2696	0.5626	0.0552	0.0960	17.61	1	14.5604	29.7919	2.0299	4.5770	21.07	-3.46	-19.66
87	0.3024	0.5627	0.0492	0.0744	28.45	1	16.2146	29.693	2.523	3.5426	27.41	1.04	3.67
88	0.311	0.5438	0.0615	0.0742	28.69	1	16.6464	28.6474	3.1472	3.527	29.70	-1.01	-3.52
89	0.3255	0.5041	0.0851	0.0753	29.68	1	17.4371	26.5614	4.3541	3.579	31.33	-1.65	-5.55
90	0.3367	0.4811	0.1009	0.0753	30.26	1	17.9677	25.2505	5.1396	3.5634	31.33	-1.07	-3.54
91	0.2905	0.5537	0.0402	0.0717	27.59	1	16.2771	29.719	2.5126	3.4697	27.72	-0.13	-0.46
92	0.2754	0.5344	0.0654	0.1002	18.31	1	15.0234	20.5694	3.3065	4.7754	22.15	-3.84	-20.95
93	0.2006	0.4903	0.0070	0.1004	18.69	1	15.7517	26.6498	4.5465	4.7050	23.77	-5.08	-27.18
94	0.3034	0.4600	0.112	0.1056	20.11	1	16.4591	24.4754	5.7534	4.9939	22.79	-2.68	-13.31
97	0.20	0.5151	0.0773	0.1006	18.63	1	15.3147	27.6018	4.0107	4.8066	22.94	-4.31	-23.12
98	0.2930	0.4777	0.0994	0.1013	19.13	1	16.0090	25.6251	5.1604	4.8431	23.64	-4.51	-23.56

TABLE B-1

Model S3-T2 Fit to all 250 C data (S385 250)

Residual Sum of Squares = 1029.57
Average Absolute Error per Observation = 12.87 %

B0 = 4.7315 B2 = 0.446
B1 = 1.2201 B3 = 0.2676

Obs. #	YH2	YCO	YCO2	YCH3OH	MEAS. RATE	DATA WT	FH2	FCO	FCO2	FCH3OH	PRED RATE	RESID.	% ERROR
99	0.3162	0.5173	0.0704	0.0723	28.33	1	17.1710	27.6530	3.6510	3.4053	31.25	-2.92	-10.29
100	0.325	0.4835	0.0901	0.0733	29.25	1	17.7380	25.950	4.6974	3.5478	31.61	-2.36	-8.06
101	0.2579	0.5077	0.1487	0.0661	24.45	0.2308	14.0454	27.118	7.6834	3.1524	26.22	-1.77	-7.26
102	0.2232	0.5055	0.154	0.0933	16.4	1	12.2455	27.092	7.9643	4.4165	14.89	1.51	9.20
103	0.2207	0.5009	0.1575	0.0925	16.28	0.2143	12.1779	26.9828	8.1827	4.3957	14.59	1.69	10.38
104	0.2392	0.5002	0.1556	0.0751	27.24	0.2308	13.1923	26.9984	8.1099	3.5998	21.93	5.31	19.51
109	0.2722	0.5667	0.0297	0.1012	18.83	1	14.9193	30.4681	1.545	4.8587	16.99	1.84	9.77
110	0.3066	0.5683	0.0240	0.0697	26.39	1	16.7556	30.6034	1.2953	3.3917	22.72	3.67	13.90
111	0.3045	0.5675	0.025	0.0705	26.64	1	16.6724	30.6242	1.3109	3.4437	22.57	4.07	15.28
112	0.2759	0.5658	0.0293	0.0947	17.43	1	15.1794	30.5618	1.5346	4.583	10.25	-0.82	-4.69
113	0.3084	0.5664	0.025	0.0705	26.72	1	16.8389	30.4705	1.3057	3.4333	22.00	3.84	14.37
114	0.2483	0.4535	0.1954	0.0663	24.06	1	13.7333	24.5534	10.2167	3.194	21.48	2.58	10.70
115	0.2264	0.4491	0.2031	0.0703	13.8	1	12.6409	24.4858	10.6745	3.7767	15.81	-2.01	-14.58
116	0.1987	0.6519	0.0527	0.0717	13.46	1	10.8306	34.8794	2.7311	3.4281	15.36	-1.90	-14.10
117	0.2047	0.6652	0.0423	0.0716	13.63	1	11.0595	35.28	2.1744	3.3917	14.57	-0.94	-6.87
118	0.228	0.6593	0.0372	0.0502	22.8	1	12.3131	35.0251	1.9195	2.7779	18.76	4.04	17.74
119	0.23	0.6534	0.0372	0.0573	22.64	1	12.4796	34.8846	1.9247	2.7519	19.25	3.39	14.99
120	0.2337	0.6373	0.049	0.0601	23.97	1	12.6565	33.9431	2.5334	2.8767	21.93	2.04	8.50
121	0.2458	0.6024	0.0696	0.0629	25.5	1	13.3119	32.0703	3.5894	3.0068	25.91	-0.41	-1.60
122	0.2593	0.5749	0.0848	0.0635	26.11	1	14.0194	30.5513	4.3697	3.0328	28.31	-2.20	-8.41
123	0.2032	0.655	0.0428	0.0695	13.22	1	11.2155	35.1447	2.2265	3.3345	15.39	-2.17	-16.44
124	0.2107	0.6375	0.0535	0.073	14	1	11.4964	34.1303	2.7727	3.4905	17.21	-3.21	-22.95
125	0.2105	0.6026	0.0749	0.0784	15.29	1	11.9334	32.268	3.8807	3.7454	19.34	-4.05	-26.47
126	0.2341	0.5632	0.0906	0.0846	16.75	1	12.7189	29.9739	5.072	4.0055	20.80	-4.05	-24.20
127	0.249	0.5343	0.1155	0.005	17.24	1	13.4036	28.3405	5.9251	4.0159	22.27	-5.03	-29.18
128	0.2795	0.5263	0.1138	0.0607	25.87	1	15.1482	28.0336	5.8783	2.9079	30.53	-4.66	0.00

TABLE B-2

Model XX14 Fit to all 250 C data (S306 250)

Residual Sum of Squares = 2083.70
Average Absolute Error per Observation = 15.26

B0 = 0.5945 B2 = 0.0537 B4 = 0.2242
B1 = 0.1603 B3 = 0.0394 B5 = 0.1874

Obs.	#	YH2	YCO	YCO2	YCH3OH	MEAS. RATE	DATA WT	FH2	FCO	FCO2	FCH3OH	PRED. RATE	RESID.	% ERROR
	1	0.2593	0.4789	0.1522	0.0041	32.7	1	14.1702	25.6146	7.0654	4.0003	28.62	4.08	12.48
	2	0.2403	0.4765	0.1571	0.096	17.23	1	13.2235	25.6094	8.1463	4.5622	19.42	-2.19	-12.70
	3	0.2463	0.472	0.1586	0.0942	16.93	1	13.5304	25.3309	8.2192	4.4789	21.14	-4.21	-24.85
	4	0.2433	0.4747	0.1581	0.0968	17.34	1	13.3483	25.4378	8.1723	4.583	19.63	-2.29	-13.22
	5	0.2746	0.4772	0.1528	0.0698	53.41	1	14.9922	25.547	7.9122	3.3397	38.17	15.24	28.53
	6	0.2619	0.4876	0.128	0.0965	73.91	1	21.2476	38.3472	9.5849	6.4001	63.81	10.10	13.67
	7	0.2234	0.4765	0.159	0.1146	83.14	1	23.5403	47.9053	14.9653	9.1332	64.62	18.52	22.27
	8	0.2699	0.4843	0.1431	0.0841	77.91	1	21.695	37.8164	10.6541	5.5735	70.29	7.62	9.79
	9	0.232	0.4641	0.1587	0.1183	40.75	1	18.9272	36.6107	11.8598	7.7347	40.77	-0.02	-0.05
	16	0.2632	0.4654	0.1567	0.0811	30.65	1	14.5032	25.1101	8.1723	3.8911	30.12	0.53	1.73
	17	0.2501	0.4746	0.1357	0.1042	78.27	1	26.466	48.2162	12.9347	8.4787	83.67	-5.40	-6.90
	18	0.2641	0.4654	0.1464	0.0908	86.55	1	27.8037	47.1865	13.9548	7.449	94.39	-7.84	-9.06
	19	0.2334	0.4902	0.1122	0.126	68.56	1	24.6567	50.3528	10.6249	10.1148	70.10	-1.54	-2.24
	20	0.2123	0.4898	0.123	0.1421	49.69	1	22.626	49.6791	11.6354	11.2697	54.21	-4.52	-9.11
	25	0.3235	0.3538	0.1389	0.1023	16.78	1	17.3851	18.5815	10.0867	4.7754	24.12	-7.34	-43.74
	26	0.3348	0.3549	0.1952	0.0919	16.26	1	18.0041	18.6856	9.9358	4.3229	30.12	-13.86	-85.25
	27	0.329	0.3575	0.1921	0.0920	34.87	1	17.8012	18.9301	9.837	4.3853	29.34	5.53	15.86
	28	0.312	0.3514	0.2016	0.1105	18.98	1	16.8493	18.5191	10.2479	5.1552	19.32	-0.34	-1.79
	29	0.3116	0.3485	0.2007	0.1136	19.5	1	16.8545	18.3943	10.2167	5.306	18.23	1.27	6.52
	32	0.333	0.3516	0.1096	0.0902	33.28	1	18.1446	18.7636	9.785	4.3021	31.14	2.14	6.43
	33	0.3105	0.3478	0.1964	0.1051	18.58	1	17.0365	18.6388	10.1595	4.9939	21.34	-2.76	-14.87
	35	0.3577	0.3629	0.1833	0.0669	12.93	1	12.8627	12.8942	6.3753	2.2161	15.06	-2.13	-16.47
	36	0.2947	0.35	0.2072	0.1174	19.46	1	19.338	22.281	12.6244	6.4398	27.57	-8.11	-41.66
	37	0.3089	0.36	0.1924	0.1016	36.03	1	20.3522	23.0774	11.828	5.6558	37.91	-1.88	-5.21
	38	0.3108	0.3489	0.1967	0.1055	19.33	1	17.0157	18.6544	10.1543	5.0043	21.22	-1.89	-9.79
	41	0.3199	0.3504	0.1926	0.1052	18.38	1	17.3955	18.618	9.8038	4.9627	23.14	-4.76	-25.90
	42	0.3396	0.3583	0.1878	0.0821	30.46	1	18.4255	19.0601	9.6653	3.9119	35.96	-5.50	-18.07
	43	0.302	0.3516	0.1972	0.1084	18.78	1	16.5892	18.852	10.2011	5.1448	18.93	-0.15	-0.79
	44	0.3204	0.3502	0.1899	0.0937	33.76	1	17.5099	19.159	9.8162	4.4685	27.95	5.81	17.21
	45	0.3032	0.3542	0.1977	0.1046	18.17	1	16.636	18.9821	10.2271	4.9731	20.39	-2.22	-12.23
	48	0.3047	0.3562	0.1981	0.1055	18.4	1	16.6412	18.9925	10.1959	4.9007	20.35	-1.95	-10.61
	52	0.3031	0.353	0.198	0.1104	18.83	1	16.5632	18.826	10.1907	5.2124	18.37	0.46	2.43
	53	0.3536	0.3629	0.1828	0.0693	11.9	1	12.7471	12.9222	6.3718	2.3002	13.60	-1.70	-14.96
	56	0.3089	0.3476	0.1979	0.1006	18.76	1	16.8961	18.5607	10.1959	5.1396	19.71	-0.95	-5.05
	57	0.3356	0.3598	0.1873	0.0836	30.65	1	18.2434	19.1746	9.6601	3.9951	34.74	-4.09	-13.34
	58	0.2799	0.3497	0.203	0.1249	19.37	1	18.6224	22.5361	12.5124	6.9002	22.98	-3.61	-18.65
	59	0.3054	0.3565	0.193	0.1051	33.64	1	20.1904	22.9201	11.9089	5.8673	35.66	-2.02	-6.01
	60	0.5351	0.1646	0.0126	0.0606	25.96	1	20.4393	0.6977	0.6503	3.4905	31.23	-5.27	-20.29
	61	0.5409	0.1459	0.0137	0.0905	16.44	1	20.7775	7.6677	0.7075	4.5518	22.07	-5.63	-34.26
	62	0.5325	0.1406	0.0121	0.0924	34.42	1	37.8699	10.458	0.0284	6.1023	41.35	-6.93	-20.14
	63	0.4925	0.1513	0.0139	0.1139	21.23	1	35.0741	10.6168	0.9457	7.4	30.02	-8.79	-41.41
	64	0.5095	0.1302	0.0564	0.0936	36.21	1	27.3625	6.9107	2.9207	4.6974	30.80	5.41	14.95
	65	0.5916	0.1464	0.006	0.0659	25.63	1	31.5189	7.777	0.3121	3.3709	26.00	-0.37	-1.43

TABLE B-2

Model XX14 Fit to all 250 C data (S386 250)

Residual Sum of Squares = 2003.78
Average Absolute Error per Observation = 15.26

B0 = 0.5945 B2 = 0.0537 B4 = 0.2242
B1 = 0.1603 B3 = 0.0394 B5 = 0.1074

Obs. #	YH2	YCO	YCO2	YCH3OH	MEAS. RATE	DATA WT	FH2	FCO	FCO2	FCH3OH	PRED. RATE	RESID.	% ERROR
66	0.5375	0.1395	0.0282	0.0916	35.14	1	20.0191	7.4181	1.467	4.6194	30.06	5.08	14.46
67	0.5913	0.1451	0.0058	0.0663	25.9	1	31.6126	7.7302	0.3017	3.4021	25.44	0.46	1.77
68	0.5693	0.1445	0.0121	0.0776	30.05	1	30.4629	7.6806	0.6294	3.9535	28.48	1.57	5.21
69	0.5005	0.129	0.0934	0.0879	35.11	1	27.3781	6.8718	4.8535	4.3853	39.16	-4.05	-11.54
70	0.5946	0.1544	0.005	0.0626	23.54	1	31.675	8.2036	0.2601	3.2044	26.58	-3.04	-12.91
71	0.5602	0.1587	0.0056	0.0665	23.63	1	29.9375	8.4428	0.2913	3.4073	24.58	-0.95	-4.00
72	0.5085	0.1329	0.006	0.0071	15.67	1	31.2536	7.0175	0.3121	4.3905	17.82	-2.15	-13.73
73	0.6031	0.1731	0.005	0.0396	37.76	1	31.9871	9.1815	0.2601	2.0392	30.79	-1.03	-2.73
74	0.5966	0.1626	0.0057	0.0495	31.57	1	31.6438	8.6145	0.2965	2.5438	34.04	-2.47	-7.82
75	0.4095	0.1174	0.0598	0.1174	21.32	1	26.5406	6.2788	3.116	5.8575	13.44	7.88	36.94
76	0.5255	0.1327	0.0505	0.0973	38.22	1	27.6486	6.9083	2.9755	4.7754	31.29	6.93	18.13
77	0.5086	0.1176	0.0609	0.117	20.91	1	26.9099	6.1384	3.1004	5.7066	15.15	5.76	27.55
78	0.5383	0.1525	0.0531	0.0633	64.02	1	20.8451	8.1255	2.7675	3.22	62.76	2.06	3.18
79	0.5465	0.1458	0.0546	0.0768	52.69	1	28.6266	7.5793	2.7779	3.7923	50.41	2.28	4.32
80	0.4036	0.106	0.0607	0.1367	48.51	1	36.5627	7.8442	4.3313	9.1045	38.37	10.14	20.89
81	0.5411	0.1371	0.053	0.0908	89.47	1	39.7641	9.9519	3.7301	6.1058	91.50	-2.03	-2.27
82	0.5192	0.125	0.057	0.1093	74	1	38.5328	9.1262	4.0271	7.3082	68.27	5.73	7.74
83	0.4078	0.1007	0.0641	0.1406	24.53	1	36.5627	7.3806	4.5269	9.2638	35.27	-10.74	-43.78

Program listing for SAS non-linear regression

```
/**/
/********\psas\xx14comm.sas***********/
/**/
libname save '\psas\';
/* *****Call non-linear regression procedure*****/
proc nlin
  data=save.s386_250
  method=marquardt;
  /****Initial parameter estimates******/
  parms b0=0 to 1 by 0.5
        b1=0 to 1 by 0.5
        b2=0 to 1 by 0.5
        b3=0 to 1 by 0.5
        b4=0 to 1 by 0.5
        b5=0 to 1 by 0.5;
  /****Define model*****/
  ka=0.001802;
  t1=(fH2**.5)*fCO-fCH3OH/(ka*fH2**1.5);
  t2=(fH2**2)*fCO2-fCO2*fCH3OH/(ka*fCO);
  t3=1+b2*fCH3OH+b3*fCO2*fH2/fCO;
  t4=1+b4*fCO2+b5*fCH3OH;
  model Rate=b0*t1/t3**2.0+b1*t2/t4**2.0;
  _weight_=Data_wt;
  /****Define parameter constraints****/
  bounds b0>=0.0,
         b1>=0.0,
         b2>=0.0,
         b3>=0.0,
         b4>=0.0,
         b5>=0.0;
  /****Partial derivatives w.r.t. parameters****/
  der.b0=t1/t3**2.0;
  der.b1=t2/t4**2.0;
  der.b2=-2*b0*t1*fCH3OH/t3**3.0;
  der.b3=-2*b0*t1*(fCO2*fH2/fCO)/t3**3.0;
  der.b4=-2*b1*t2*fCO2/t4**3.0;
  der.b5=-2*b1*t2*fCH3OH/t4**3.0;
  /*****Set up output**********/
  output out=save.xx146250 p=pred r=resid parms=b0 b1 b2 b3 b4 b5
                           sse=sumsqs;
run;
/********Print results to screen********/
proc print data=save.xx146250;
  title 'Model XX14 fit to All Data (S386_250)';
  title2 '     ';
run;
```

END

DATE
FILMED
02/11/92

I